



# Thermoelastic Dissipation in Vibrations of Couple Stress-Based Circular Cross-sectional Beams with Nonlocal Single-Phase-Lag Heat Conduction

Younus Fahad Breesam<sup>1</sup> · Sherzod Shukhratovich Abdullaev<sup>2,3</sup> · Raed H. Althomali<sup>4</sup> · F. Al-dolaimy<sup>5</sup> · M. K. Sharma<sup>6</sup> · Muataz S. Alhassan<sup>7</sup> · Ahmed Hussien Alawadi<sup>10,8,9</sup> · Ali Alsaalamy<sup>11</sup> · Kadhim Abbas Jabbar<sup>12</sup>

Received: 15 November 2023 / Revised: 30 January 2024 / Accepted: 25 March 2024

© Springer Nature Singapore Pte Ltd. 2024

## Abstract

**Purpose** Given the need for utilizing size-dependent elasticity theories and non-Fourier heat transfer models in extremely small dimensions, the present research intends to provide a novel theoretical framework for thermoelastic dissipation (TED) in circular cross-sectional micro/nanobeams on the basis of the modified couple stress theory (MCST) and nonlocal single-phase-lag (NSPL) heat conduction model.

**Methods** In the first step, the coupled heat equation of Euler–Bernoulli beams in polar coordinate system is derived by capturing the nonlocal and phase-lagging effects. By solving this equation, the function of temperature change is attained. Substitution of the couple stress-based constitutive relations and obtained temperature field in the definition of TED from the point of view of energy yields a TED relation in the form of infinite series encompassing mechanical length scale, thermal nonlocal and phase lag parameters.

**Results** Numerical results are provided in three sections. In the first section, the correctness of the extracted formulation is explored via conducting a comparative study. In the second section, a convergence analysis is performed to ascertain the sufficient number of terms of the obtained infinite series for achieving well-founded outcomes. In the final section, a parametric analysis is made to illuminate the dependence of TED on some factors like mechanical length scale parameter, thermal nonlocal parameter, beam geometry, ambient temperature and beam material.

**Conclusion** According to the obtained results, utilization of MCST lowers the amount of TED. Moreover, the incorporation of thermal nonlocal parameter in the governing equations can have substantial impacts on both the amount and the trend of TED, especially at high vibration frequencies.

**Keywords** Circular cross-sectional micro/nanobeams · Thermoelastic dissipation · Scale-dependent analysis · Modified couple stress theory · Nonlocal single-phase-lagging effect · Theoretical approach

## Background

Micro/nano-electromechanical systems (MEMS/NEMS) can be incredibly little, with some segments measuring no more than a few nanometers in size. This makes them perfect for utilizing in applications where space is restricted, such as in consumer electronics, medical equipment, and aerospace devices [1–5]. In addition, advantages such as low cost, little power consumption, high accuracy and versatility have made MEMS/NEMS attractive options for use in industrial and engineering applications. For instance, MEMS and NEMS devices are exploited in flow sensors [6, 7], gyroscopes [8–10], pressure sensors [11, 12], accelerometers [13, 14], temperature sensors [15, 16] and microfluidic devices [17]. MEMS and NEMS technology is still under development. As MEMS and NEMS devices become smaller, cheaper, and more powerful, they are likely to be employed in even more engineering applications in the future.

The findings from various experimental tests reveal that the static and dynamic responses of small-sized structural elements are influenced by their size. The classical theory (CT) of elasticity is inadequate in representing this aspect of micro/nanostructures as its constitutive equations lack length scale parameters. To overcome this limitation of CT, several elasticity theories that account for scale effect and comprise one or more length scale parameters have been proposed [18–23]. In the couple stress theory (CST) [18], two additional characteristic lengths have been incorporated to consider the influence of size in the constitutive relations. Yang et al. [19] established the modified couple stress theory (MCST), which introduces a single length scale parameter into the governing equations by making specific amendments to CST. As a consequence, the couple stress tensor becomes symmetric, leading to a substantial simplification in its application. To examine the impact of size on the mechanical characteristics of micro/nanostructures, numerous analytical studies have been performed employing various size-dependent elasticity theories [24–33]. For instance, Sladek et al. [34] utilized the strain gradient theory (SGT) to create a mathematical framework for describing the size-dependent characteristics of in-plane cracks in piezoelectric nanostructures under thermal loading.

An important part of MEMS and NEMS devices consists of structures like beams, rings, disks and plates [35–38]. The Fourier heat conduction model is based on the assumption that the heat flux at a point is proportional to the temperature gradient at that point. This assumption is valid for macroscopic systems, but it fails at micron and submicron dimensions. This is because the mean free path of phonons can be comparable to the size of the system

at small scales. Non-Fourier heat conduction models capture the non-diffusive transport of phonons at small scales. These models are typically more complex to solve than the Fourier model, but they can be used to design and optimize micro/nanostructures for a variety of applications. Among the most significant non-Fourier models, one can cite single-phase-lag (SPL) [39], Green–Naghdi (GN) [40], Green–Lindsay (GL) [41], Moore–Gibson–Thompson (MGT) [42], dual-phase-lag (DPL) [43] and nonlocal single-phase-lag (NSPL) [44] models. In addition to the mentioned models, by taking into account the second derivatives of temperature within the constitutive equation for the higher-order heat flux, Sladek et al. [45] formulated an innovative gradient theory to characterize nonlocal heat conduction in nanostructures. With the help of different models introduced for heat transfer, numerous articles have been published on thermomechanical responses of thermoelastic media and structures [46–60].

Thermoelastic dissipation (TED) is a phenomenon where the mechanical energy of an oscillating structure is dissipated as heat owing to the internal friction induced by the temperature variations in the material. This is caused by the thermal expansion and contraction of the structure as it vibrates. TED can be remarkable in micro/nanoscale devices, where other sources of damping like viscous damping and Coulomb damping are mostly inconsequential. TED is a principal reason for energy loss in MEMS/NEMS and can affect their performance and reliability. Consequently, it is important to understand and model TED when designing micro/nanoscale systems. The earliest mathematical framework for TED has been established by Zener [61], in which he employed the classical theory (CT) of elasticity and the Fourier law, and achieved an analytical TED relation for slender beams in the context of energy approach. By using another approach called the frequency approach, Lifshitz and Roukes [62] derived a simpler expression for TED in classical Euler–Bernoulli beams. By means of energy and frequency approaches, and employing different elasticity theories and heat conduction models, many researchers have worked on the modeling of TED in small-sized mechanical devices, which are introduced below a selection of these studies.

By utilizing DPL model and extracting a size-dependent formula for TED, Guo et al. [63] evaluated the influence of phase lag parameters on TED in micro/nanobeam resonators. By using energy approach, Zhou et al. [64] and Zhou et al. [65] presented analytical solutions for TED in small-scaled circular cross-sectional beams on the basis of SPL and DPL models, respectively. According to CT and the Fourier model, Zuo et al. [66] developed a theoretical framework for computing TED value in anisotropic piezoelectric microbeam resonators. Based on DPL model, Kim and Kim [67] established a mathematical

formulation to illuminate the impact of phase lags on TED in micro/nanorings with circular cross section. In the context of CT and the Fourier model, Zheng et al. [68] implemented Rayleigh–Ritz method to attain an analytical solution for TED in small-sized tubular shells with arbitrary boundaries. Kumar and Mukhopadhyay [69] provided a mathematical formulation on the basis of nonlocal theory (NT), modified couple stress theory (MCST) and MGT model to estimate the amount of TED in nanobeam resonators. By accounting for surface effect and exploiting DPL model, Shi et al. [70] established a size-dependent TED model for nanobeams. Borjalilou and Asghari [71] employed MCST and DPL model to highlight size effect on TED variations in miniaturized rectangular plates. Within the framework of MCST and the Fourier law, Yang et al. [72] rendered a theoretical model for TED in rectangular micro/nanoplates with three-dimensional (3D) heat conduction. With the aid of MCST and nonlocal dual-phase-lag model, Ge and Sarkar [73] developed a comprehensive model to assess TED in rectangular cross-sectional micro/nanoring resonators. In addition to the mentioned cases, many other papers have been published in the field of TED calculation by analytical method in different structures [74–89].

The aforementioned content highlights that, up until now, TED modeling in micro/nanobeam resonators with circular cross section has been conducted solely in the framework of SPL and DPL heat conduction models, utilizing the classical theory of elasticity and without accounting for the size effect in the structural domain. The current paper strives to establish a mathematical framework for predicting TED value in small-scaled circular cross-sectional beams using the modified couple stress theory (MCST) and nonlocal single-phase-lag (NSPL) model for the first time. To attain this target, the coupled heat equation of Euler–Bernoulli beams on the basis of NSPL model is firstly extracted in polar coordinates. This differential equation is then solved to determine the temperature field in the beam. By inserting the constitutive relations and obtained temperature field in the definition of TED in the context of the energy approach, a NSPL-based mathematical relationship for TED is derived in the form of infinite series. In the numerical results section, the validity of provided model is firstly surveyed by making a comparative analysis. After that, with the aim of finding out the adequate number of terms of the solution for achieving reliable results, a convergence study is accomplished. Eventually, via a thorough parametric study, the sensitivity of TED to some crucial factors such as thermal nonlocal parameter, size of beam, environment temperature and material is analyzed.

## Problem Formulation

### Basic Relations of Nonlocal Single-Phase-Lag Heat Conduction Model

Based on the nonlocal single-phase-lag (NSPL) generalized thermoelasticity theory [44, 64], the equation of heat conduction can be expressed via the following relation:

$$\left(1 + \tau \frac{\partial}{\partial t} - l_Q^2 \nabla^2\right) \mathbf{q} = -k \nabla \theta \quad (1)$$

In the above equation,  $\mathbf{q}$  represents the vector of heat flux. Moreover, symbol  $\theta = T - T_0$  is the temperature increment, in which parameters  $T$  and  $T_0$  denote the instantaneous and reference temperatures, respectively. Variable  $t$  represents time. Parameter  $k$  refers to the thermal conductivity of material. Non-classical constants  $\tau$  and  $l_Q$  stand for phase lag and thermal nonlocal parameters, respectively. Note that by eliminating parameter  $l_Q$  from Eq. (1), this equation becomes the constitutive relation of SPL model. Furthermore, when both parameters  $\tau$  and  $l_Q$  are set to zero, the NSPL-based heat equation is converted to the heat equation of Fourier law.

The equation of conservation of energy is given by [44]:

$$\nabla \cdot \mathbf{q} = -\rho c_v \frac{\partial \theta}{\partial t} - \frac{E \alpha T_0}{1 - 2\nu} \frac{\partial \epsilon_c}{\partial t} \quad (2)$$

in which material constants  $\rho$  and  $c_v$  represent mass density and specific heat per unit mass, respectively. Moreover, symbol  $\alpha$  defines thermal expansion coefficient of the material. Parameters  $E$  and  $\nu$  denote the Young modulus and Poisson ratio, respectively. Variable  $\epsilon_c$  stands for the cubical strain which is equal to the trace of strain tensor  $\epsilon$ . The omission of heat flux vector  $\mathbf{q}$  from Eqs. (1) and (2) provides:

$$k \nabla^2 \theta = \left(1 + \tau \frac{\partial}{\partial t} - l_Q^2 \nabla^2\right) \left(\rho c_v \frac{\partial \theta}{\partial t} + \frac{E \alpha T_0}{1 - 2\nu} \frac{\partial \epsilon_c}{\partial t}\right) \quad (3)$$

### Basic Relations of Modified Couple Stress Theory

According to the modified couple stress theory (MCST), the strain energy  $U$  of an elastic body encompassing volume  $\Omega$  is expressed by [19]:

$$U = \frac{1}{2} \iiint_{\Omega} \left(\sigma_{ij} \epsilon_{ij} + m_{ij} \gamma_{ij}^s\right) d\Omega \quad (4)$$

In the above equation,  $\sigma_{ij}$  and  $m_{ij}$  denote the components of Cauchy stress tensor  $\boldsymbol{\sigma}$  and deviatoric part of couple stress tensor  $\mathbf{m}$ , respectively. Additionally, symbols  $\epsilon_{ij}$  and  $\gamma_{ij}^s$  refer to the components of strain tensor  $\boldsymbol{\epsilon}$  and the symmetric part of

rotation gradient tensor  $\gamma^s$ , respectively. The mathematical relations of these kinematic parameters are given by:

$$\epsilon_{ij} = \frac{1}{2} \left( \frac{\partial u_i}{\partial x_j} + \frac{\partial u_j}{\partial x_i} \right) \tag{5a}$$

$$\gamma_{ij}^s = \frac{1}{2} \left( \frac{\partial \varphi_i}{\partial x_j} + \frac{\partial \varphi_j}{\partial x_i} \right) \text{ where } \varphi_i = \frac{1}{2} (\text{curl}(\mathbf{u}))_i \tag{5b}$$

in which  $\mathbf{u}$  represents the displacement vector, and  $u_i$  stands for its components. Moreover, variable  $\varphi_i$  denotes the components of rotation vector  $\Phi$ . The non-classical constitutive relations in the context of MCST are expressed by:

$$m_{ij} = 2\mu l_M^2 \gamma_{ij}^s \tag{6}$$

where  $l_M$  is the mechanical length scale parameter. Furthermore, parameter  $\mu$  denotes the shear modulus, which is obtained via the following relation:

$$\mu = \frac{E}{2(1 + \nu)} \tag{7}$$

### Coupled Thermoelastic Constitutive Relations of Circular Cross-sectional Beams

Geometry and coordinate system of a circular cross-sectional beam with radius  $a$  and length  $L$  are demonstrated in Fig. 1. The beam coordinate system is represented by  $(x, y, z)$  in the Cartesian system and  $(x, r, \beta)$  in the cylindrical system. In the Cartesian system, the displacement field of an Euler–Bernoulli beam is described via the following relations:

$$u_x = -z \frac{\partial w(x, t)}{\partial x}, u_y = 0, u_z = w(x, t) \tag{8}$$

where  $u_x, u_y$  and  $u_z$  are displacements along the directions  $x, y$  and  $z$ , respectively. Also, function  $w(x, t)$  represents lateral

deflection of the beam. According to Eq. (8), normal strain  $\epsilon_{xx}$  can be obtained as follows [64]:

$$\epsilon_{xx} = -z \frac{\partial^2 w}{\partial x^2} \tag{9}$$

Coupled thermoelastic constitutive relations are expressed by [77]:

$$\epsilon_{ij} = \frac{1}{E} [(1 + \nu)\sigma_{ij} - \nu\sigma_{kk}\delta_{ij}] + \alpha\theta\delta_{ij} \tag{10}$$

in which  $\epsilon_{ij}$  and  $\sigma_{ij}$  denote the components of strain tensor  $\epsilon$  and stress tensor  $\sigma$ , respectively. Moreover,  $\sigma_{kk}$  refers to the trace of tensor  $\sigma$ . Parameter  $\delta_{ij}$  stands for the components of the Kronecker delta. By considering the uniaxial state of stress in thin beams (i.e.  $\sigma_{yy} = \sigma_{zz} = 0$ ), Eq. (10) leads to the relation below:

$$\sigma_{xx} = E\epsilon_{xx} - E\alpha\theta \tag{11}$$

By substituting the above equation into Eq. (10), one can get:

$$\epsilon_{yy} = \epsilon_{zz} = -\nu\epsilon_{xx} + (1 + \nu)\alpha\theta \tag{12}$$

Hence, the cubical strain  $\epsilon_c$  can be obtained as follows:

$$\epsilon_c = \epsilon_{xx} + \epsilon_{yy} + \epsilon_{zz} = (1 - 2\nu)\epsilon_{xx} + 2(1 + \nu)\alpha\theta \tag{13}$$

By inserting Eq. (9) into the above equation, the following relation is derived:

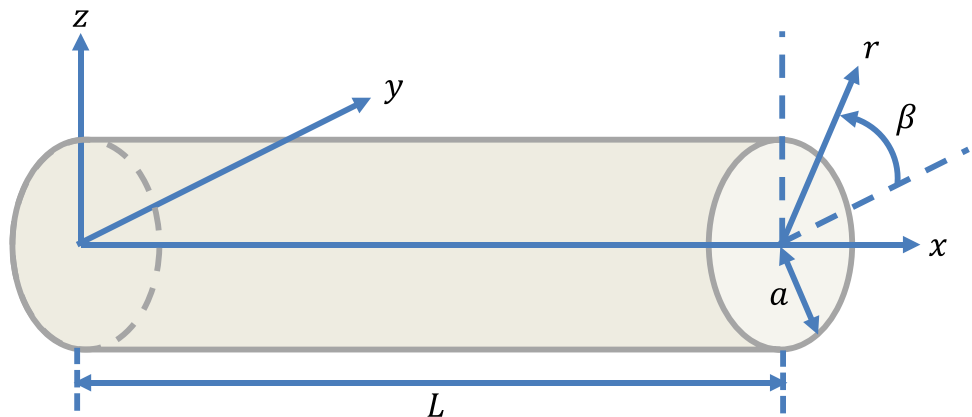
$$\epsilon_c = -(1 - 2\nu)z \frac{\partial^2 w}{\partial x^2} + 2(1 + \nu)\alpha\theta \tag{14}$$

Substitution of Eq. (8) into Eq. (5b) yields the following relation:

$$\gamma_{xy}^s = \gamma_{yx}^s = -\frac{1}{2} \frac{\partial^2 w}{\partial x^2} \tag{15}$$

By inserting the above equation into Eq. (6), one can obtain:

**Fig. 1** Configuration and coordinate system of a circular cross-sectional beam resonator



$$m_{xy} = m_{yx} = -\mu l_M^2 \frac{\partial^2 w}{\partial x^2} \tag{16}$$

**NDPL-Based Heat Equation of Circular Cross-sectional Beams**

By substituting Eq. (14) into Eq. (3) and simplifying the result, one can arrive at the following equation:

$$k \nabla^2 \theta = \left( 1 + \tau \frac{\partial}{\partial t} - l_Q^2 \nabla^2 \right) \times \left[ \rho c_v \frac{\partial \theta}{\partial t} \left( 1 + \frac{2(1 + \nu)}{1 - 2\nu} \Delta_Z \right) - E \alpha T_0 z \frac{\partial^2 w}{\partial x^2 \partial t} \right] \tag{17}$$

in which

$$\Delta_Z = \frac{E \alpha^2 T_0}{\rho c_v} \tag{18}$$

In most cases,  $\Delta_Z \ll 1$ . Therefore, Eq. (17) can be expressed in the following form:

$$k \nabla^2 \theta = \left( 1 + \tau \frac{\partial}{\partial t} - l_Q^2 \nabla^2 \right) \left[ \rho c_v \frac{\partial \theta}{\partial t} - E \alpha T_0 z \frac{\partial^2 w}{\partial x^2 \partial t} \right] \tag{19}$$

By introducing  $\chi = k/\rho c_v$ , the above equation can be written as follows:

$$\chi \nabla^2 \theta - \frac{\partial}{\partial t} \left( 1 + \tau \frac{\partial}{\partial t} - l_Q^2 \nabla^2 \right) \theta = - \frac{\partial}{\partial t} \left( 1 + \tau \frac{\partial}{\partial t} - l_Q^2 \nabla^2 \right) \frac{\Delta_Z z}{\alpha} \frac{\partial^2 w}{\partial x^2} \tag{20}$$

To solve the above partial differential equation, the following simple harmonic forms are adopted for temperature increment  $\theta$  and lateral deflection  $w$ :

$$\theta(x, y, z, t) = \Theta(x, y, z) e^{i\omega t} = \Theta(x, r, \beta) e^{i\omega t} \tag{21a}$$

$$w(x, t) = W(x) e^{i\omega t} \tag{21b}$$

where  $\omega$  stands for the vibrational frequency of the beam. Substitution of Eqs. (21a) and (21b) into Eq. (20) results in the following equation:

$$\chi \nabla^2 \Theta - i\omega \left( 1 + i\omega\tau - l_Q^2 \nabla^2 \right) \Theta = -i\omega \left( 1 + i\omega\tau - l_Q^2 \nabla^2 \right) \frac{\Delta_Z z}{\alpha} \frac{d^2 W}{dx^2} \tag{22}$$

Considering that  $\nabla^2 = (\partial^2/\partial y^2) + (\partial^2/\partial z^2)$ , the above equation can be expressed in the following form:

$$\nabla^2 \Theta - \frac{1}{\chi} \frac{i\omega - \tau\omega^2}{1 + i\omega\tau_N} \Theta = - \frac{\Delta_Z}{\alpha} \frac{1}{\chi} \frac{i\omega - \tau\omega^2}{1 + i\omega\tau_N} z \frac{d^2 W}{dx^2} \text{ where } \tau_N = \frac{l_Q^2}{\chi} \tag{23}$$

According to Fig. 1, one can write:

$$y = r \cos \beta, z = r \sin \beta \tag{24}$$

Hence, Eq. (23) can be written in polar coordinate as follows:

$$\nabla^2 \Theta - \frac{1}{\chi} \frac{i\omega - \tau\omega^2}{1 + i\omega\tau_N} \Theta = - \frac{\Delta_Z}{\alpha} \frac{1}{\chi} \frac{i\omega - \tau\omega^2}{1 + i\omega\tau_N} \frac{d^2 W}{dx^2} r \sin \beta \tag{25}$$

where the Laplacian operator in polar coordinate has the following form:

$$\nabla^2 = \frac{\partial^2}{\partial r^2} + \frac{1}{r} \frac{\partial}{\partial r} + \frac{1}{r^2} \frac{\partial^2}{\partial \beta^2} \tag{26}$$

**Temperature Distribution in the Circular Cross-Sectional Beam**

According to Eq. (26), it can be concluded that the partial differential Eq. (25) is a Bessel type equation with respect to  $r$ . Therefore, the solution of Eq. (25) can be expressed as follows:

$$\Theta = \sum_{i=0}^{\infty} \sum_{j=1}^{\infty} J_i \left( \frac{\lambda_{ij}}{a} r \right) [A_{ij} \sin(i\beta) + B_{ij} \cos(i\beta)] \tag{27}$$

where  $J_i$  represents  $i$ th-order Bessel function of the first kind. In addition,  $A_{ij}$ ,  $B_{ij}$  and  $\lambda_{ij}$  are unknown constants that must be determined. Given no extension or contraction in the neutral plane, temperature amplitude in this plane should be zero. Consequently, for  $i\beta = n\pi$  ( $n = 1, 2, 3, \dots$ ), we have  $B_{ij} = 0$ . In addition, by considering the right side of Eq. (25) and orthogonality property of trigonometric functions, one can infer that  $A_{ij} = 0$  for  $i \neq 1$ . Given these points, Eq. (27) can be written in the following simpler form:

$$\Theta = \sin \beta \sum_{j=1}^{\infty} A_{1j} J_1 \left( \frac{\lambda_{1j}}{a} r \right) \tag{28}$$

It is assumed that the surface of the beam is thermally insulated. By referring to Eq. (21a), one can deduce that  $\partial \Theta / \partial r = 0$  at  $r = a$ . This means that:

$$\frac{\partial}{\partial r} \left( J_1 \left( \frac{\lambda_{1j}}{a} r \right) \right) = 0 \text{ at } r = a \tag{29}$$

Based on the properties of Bessel functions, one can write:

$$\frac{\partial}{\partial r} (J_1(\delta r)) = \delta J_0(\delta r) - \frac{1}{r} J_1(\delta r) \tag{30}$$

By setting  $\delta = \lambda_{1j}/a$  and utilizing the above equation in Eq. (29), one can reach the following characteristic equation to determine the value of  $\lambda_{1j}$ :

$$\lambda_{1j} J_0(\lambda_{1j}) - J_1(\lambda_{1j}) = 0 \tag{31}$$

Note that according to the properties of Bessel functions, the above equation is equivalent to equation  $J_0(\lambda_{1j}) - J_2(\lambda_{1j}) = 0$  and their roots are the same. The first ten roots of Eq. (31) can be seen in Table 1. By substituting Eq. (28) into Eq. (25) and grouping similar terms, one can get:

$$\sum_{j=1}^{\infty} A_{1j} J_1\left(\frac{\lambda_{1j}}{a} r\right) \left[ \left(\frac{\lambda_{1j}}{a}\right)^2 + \frac{i\omega - \tau\omega^2}{\chi(1 + i\omega\tau_N)} \right] = \frac{\Delta_Z}{\alpha} \frac{i\omega - \tau\omega^2}{\chi(1 + i\omega\tau_N)} \frac{d^2 W}{dx^2} r \tag{32}$$

At this stage, we use the orthogonality property of Bessel functions as follows to determine the coefficient  $A_{1j}$ :

$$\int_0^a r J_1\left(\frac{\lambda_{1j}}{a} r\right) J_1\left(\frac{\lambda_{1i}}{a} r\right) dr = \begin{cases} 0 & i \neq j \\ \frac{a^2}{2} \left(\frac{\lambda_{1j}^2 - 1}{\lambda_{1j}^2}\right) (J_1(\lambda_{1j}))^2 & i = j \end{cases} \tag{33}$$

Moreover, we have:

$$\int_0^a r^2 J_1\left(\frac{\lambda_{1j}}{a} r\right) dr = \frac{a^3}{\lambda_{1j}^2} J_1(\lambda_{1j}) \tag{34}$$

Hence, by multiplying the sides of Eq. (32) by  $r J_1\left(\frac{\lambda_{1j}}{a} r\right)$ , integrating the result from 0 to  $a$ , and using Eqs. (33) and (34), the coefficient  $A_{1j}$  is finally obtained as follows:

$$A_{1j} = 2a \frac{\Delta_Z}{\alpha} \frac{d^2 W}{dx^2} \frac{1}{(\lambda_{1j}^2 - 1) J_1(\lambda_{1j})} \frac{i\omega\tau_j - \tau\tau_j\omega^2}{(1 - \tau\tau_j\omega^2) + i\omega(\tau_N + \tau_j)} \tag{35}$$

with

$$\tau_j = \frac{a^2}{\chi \lambda_{1j}^2} \tag{36}$$

Therefore, according to Eqs. (28) and (35), temperature amplitude  $\Theta$  can be expressed as follows:

$$\Theta(x, r, \beta) = 2a \frac{\Delta_Z}{\alpha} \frac{d^2 W}{dx^2} \sin\beta \sum_{j=1}^{\infty} \frac{1}{(\lambda_{1j}^2 - 1) J_1(\lambda_{1j})} \frac{i\omega\tau_j - \tau\tau_j\omega^2}{(1 - \tau\tau_j\omega^2) + i\omega(\tau_N + \tau_j)} J_1\left(\frac{\lambda_{1j}}{a} r\right) \tag{37}$$

### Derivation of TED Relation

To calculate the amount of TED in mechanical structures, the inverse of quality factor (Q-factor) is used. In the context of energy approach, TED value is computed via the following relation [64]:

$$Q^{-1} = \frac{1}{2\pi} \frac{\Delta E}{E_{max}} \tag{38}$$

in which  $\Delta E$  and  $E_{max}$  represent the dissipated thermoelastic energy and the maximum amount of strain energy per cycle of oscillation, respectively. In an elastic body with volume  $\Omega$ , the amount of  $\Delta E$  and  $E_{max}$  can be estimated by [73]:

$$\Delta E = -\pi \iiint_{\Omega} \hat{\sigma}_{ij} Im(\hat{\epsilon}_{ij}^{th}) d\Omega \text{ with } \epsilon_{ij}^{th} = \alpha\theta\delta_{ij} \tag{39a}$$

$$E_{max} = \frac{1}{2} \iiint_{\Omega} (\hat{\sigma}_{ij}\hat{\epsilon}_{ij} + \hat{m}_{ij}\hat{\gamma}_{ij}^s) d\Omega \tag{39b}$$

In the above relations, the hat symbol on each variable denotes the highest amount of that variable in one cycle of oscillation. Additionally,  $\epsilon_{ij}^{th}$  indicates thermal strain. Moreover, the operator  $Im$  stands for the imaginary part of different parameters. For a beam, one can write:

$$\Delta E = -\pi \iiint_{\Omega} \hat{\sigma}_{xx} Im(\hat{\epsilon}_{xx}^{th}) d\Omega \text{ with } \epsilon_{xx}^{th} = \alpha\theta \tag{40}$$

where

$$d\Omega = dr \cdot rd\beta \cdot dx \tag{41}$$

By considering Eqs. (9), (11) and (21b), and the fact that thermal stress is negligible compared to mechanical stress, one can attain:

$$\hat{\sigma}_{xx} = -Er \frac{d^2 W}{dx^2} = -Er \sin\beta \frac{d^2 W}{dx^2} \tag{42}$$

Moreover, use of Eqs. (21a) and (37) leads to:

$$Im(\hat{\epsilon}_{xx}^{th}) = \alpha Im(\Theta) = 2a \Delta_Z \frac{d^2 W}{dx^2} \sin\beta \sum_{j=1}^{\infty} \frac{1}{(\lambda_{1j}^2 - 1) J_1(\lambda_{1j})} \times \frac{\tau_j\omega + \tau\tau_j\tau_N\omega^3}{(1 - \tau\tau_j\omega^2)^2 + (\tau_j + \tau_N)^2\omega^2} J_1\left(\frac{\lambda_{1j}}{a} r\right) \tag{43}$$

**Table 1** Values of the first ten terms of  $\lambda_{1j}$  and  $C_j$

$j$	$\lambda_{1j}$	$C_j$
1	1.841	0.987
2	5.331	0.010
3	8.536	$1.528 \times 10^{-3}$
4	11.706	$4.292 \times 10^{-4}$
5	14.864	$1.647 \times 10^{-4}$
6	18.016	$7.618 \times 10^{-5}$
7	21.164	$3.996 \times 10^{-5}$
8	24.311	$2.294 \times 10^{-5}$
9	27.457	$1.409 \times 10^{-5}$
10	30.602	$9.132 \times 10^{-6}$



By substituting Eqs. (41), (42) and (43) into Eq. (40) and integrating the result over  $0 \leq r \leq a$ ,  $0 \leq \beta \leq 2\pi$  and  $0 \leq x \leq L$ , the relation of  $\Delta E$  is obtained as follows:

$$\Delta E = 2\pi^2 \Delta_Z E a^4 \sum_{j=1}^{\infty} \frac{1}{\lambda_{lj}^2 (\lambda_{lj}^2 - 1)} \times \frac{\tau_j \omega + \tau \tau_j \tau_N \omega^3}{(1 - \tau \tau_j \omega^2)^2 + (\tau_j + \tau_N)^2 \omega^2} \int_0^L \left( \frac{d^2 W}{dx^2} \right)^2 dx \tag{44}$$

According to Eq. (39b), parameter  $E_{max}$  for a beam can be written as:

$$E_{max} = \frac{1}{2} \iiint_{\Omega} \left( \hat{\sigma}_{xx} \hat{\epsilon}_{xx} + \hat{m}_{xy} \hat{\gamma}_{xy}^s + \hat{m}_{yx} \hat{\gamma}_{yx}^s \right) d\Omega \tag{45}$$

By considering Eqs. (9) and (21b), one can get:

$$\hat{\epsilon}_{xx} = -z \frac{d^2 W}{dx^2} = -r \sin \beta \frac{d^2 W}{dx^2} \tag{46}$$

Moreover, utilization of Eqs. (15), (16) and (21b) gives:

$$\hat{\gamma}_{xy}^s = \hat{\gamma}_{yx}^s = -\frac{1}{2} \frac{d^2 W}{dx^2} \tag{47a}$$

$$\hat{m}_{xy} = \hat{m}_{yx} = -\mu l_M^2 \frac{d^2 W}{dx^2} \tag{47b}$$

Substitution of Eqs. (41), (42), (46), (47a) and (47b) into Eq. (45) and integration of result in the range of the volume of beam leads to:

$$E_{max} = \frac{1}{8} \pi E a^4 \left[ 1 + 4 \frac{\mu}{E} \left( \frac{l_M}{a} \right)^2 \right] \int_0^L \left( \frac{d^2 W}{dx^2} \right)^2 dx \tag{48}$$

At last, by inserting Eqs. (44) and (48) into Eq. (38), one can achieve the following TED expression for circular cross-sectional beams according to MCST and NSPL heat conduction model:

$$Q^{-1} = \frac{\Delta_Z}{1 + 4 \frac{\mu}{E} \left( \frac{l_M}{a} \right)^2} \sum_{j=1}^{\infty} C_j \frac{\tau_j \omega + \tau \tau_j \tau_N \omega^3}{(1 - \tau \tau_j \omega^2)^2 + (\tau_j + \tau_N)^2 \omega^2} \tag{49}$$

where  $C_j$  represents the weighting coefficient defined by the following relationship:

$$C_j = \frac{8}{\lambda_{lj}^2 (\lambda_{lj}^2 - 1)} \tag{50}$$

The values of sequence  $C_j$  for its first ten terms are given in Table 1. As can be seen, the value of the terms of sequence

$C_j$  shrinks rapidly. By referring to Eq. (7), the TED relation in Eq. (49) can be expressed as follows:

$$Q^{-1} = \frac{\Delta_Z}{R} \sum_{j=1}^{\infty} C_j \frac{\tau_j \omega + \tau \tau_j \tau_N \omega^3}{(1 - \tau \tau_j \omega^2)^2 + (\tau_j + \tau_N)^2 \omega^2} \text{ with } R = 1 + \frac{2}{1 + \nu} \left( \frac{l_M}{a} \right)^2 \tag{51}$$

Considering that the TED relation in Eq. (51) is an infinite series, it is necessary to account for a finite number of terms of the mentioned relation to extract the numerical results. For this reason, the relationship of TED, including its first  $n$  terms, can be shown as follows:

$$Q_n^{-1} = \sum_{j=1}^n q_j^{-1} \text{ with } q_j^{-1} = \frac{\Delta_Z}{R} C_j \frac{\tau_j \omega + \tau \tau_j \tau_N \omega^3}{(1 - \tau \tau_j \omega^2)^2 + (\tau_j + \tau_N)^2 \omega^2} \tag{52}$$

Indeed, in the above equation,  $q_j^{-1}$  represents the  $j$ -th mode of thermoelastic dissipation.

## Numerical Results and Discussions

### Model Validation

To assess the correctness of established model, the outcomes of this work are compared with those extracted by Zhou et al. [64] on the basis of classical elasticity theory and SPL model. Note that to derive the results in the framework of CT and SPL model, it is enough to set the values of  $l_M$  and  $l_Q$  to zero in the formulation developed in this article. In other words,  $l_M = \tau_N = 0$  should be placed in TED relationship presented in Eq. (51). By considering the abovementioned explanations, TED variations against the vibration frequency  $\omega$  is depicted in Fig. 2 for a beam with radius  $a = 100$  nm at  $T_0 = 300$  K. In this figure, curves of  $Q_1^{-1}$  and  $Q_{10}^{-1}$  are drawn. Thermomechanical properties of the beam material are:  $E = 160$  GPa,  $\rho = 2330$  kg/m<sup>3</sup>,  $c_v = 699.57$  J/kg K,  $k = 150$  W/m K,  $\alpha = 2.6 \times 10^{-6}$  1/K and  $\tau = 4.02$  ps. The perfect match between the results derived through the relation provided in this article and those reported by Zhou et al. [64] implies the validity and accuracy of the established formulation.

### Convergence Analysis

In this section, a convergence study is done to determine how many terms of TED relation in Eq. (51) can lead to a convergent and sufficiently accurate answer. To extract the

**Fig. 2** Comparison study for evaluating the validity of developed formulation with the results of Zhou et al. [64]

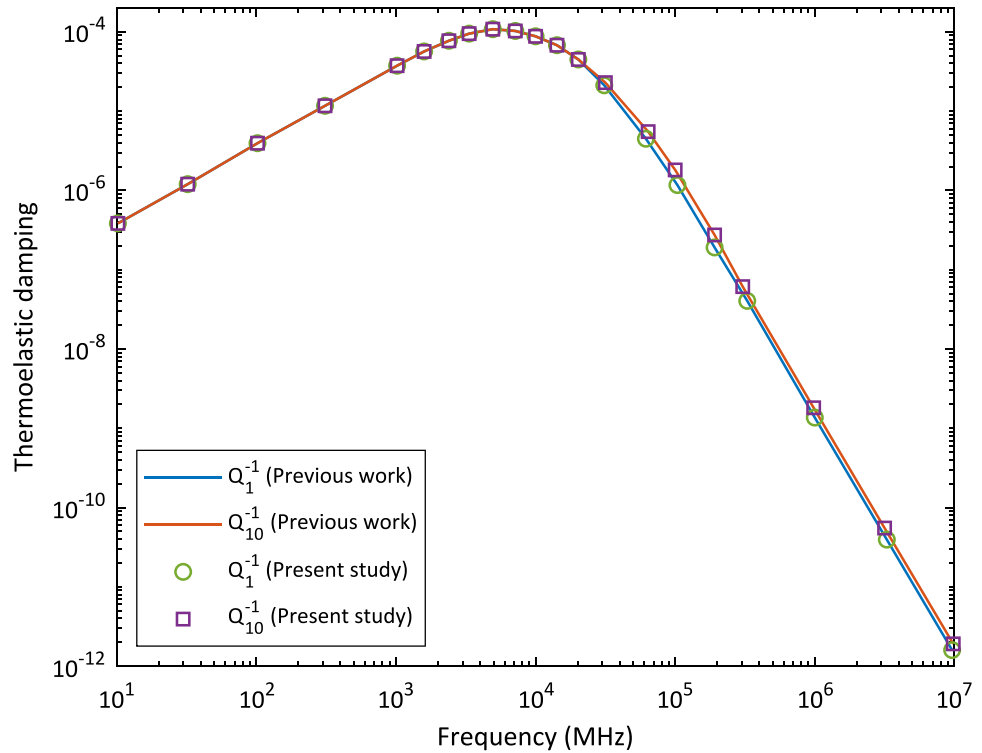


**Table 2** Thermomechanical properties of silicon, gold and diamond at reference temperature  $T_0 = 300$  K

Material	$E$ (GPa)	$\nu$	$\rho$ (kg/m <sup>3</sup> )	$k$ (W/mK)	$\rho c_v$ (J/m <sup>3</sup> K)	$\alpha$ (10 <sup>-6</sup> /K)	$\tau$ (ps)
Silicon	160	0.22	2300	150	$1.6 \times 10^6$	2.6	4.04
Gold	82	0.4	19,300	320	$2.5 \times 10^6$	15	90.4
Diamond	1070	0.18	3520	2000	$1.83 \times 10^6$	1.1	10.8

results, a silicon (Si) beam at a temperature of  $T_0 = 300$  K is considered. The material properties of silicon at the mentioned temperature are given in Table 2 [90]. By assuming  $l_M = 0.5 \mu\text{m}$  and  $l_Q = 150 \text{ nm}$ , Figs. 3a and 3b indicate the variations of thermoelastic dissipation modes  $q_1^{-1}, q_2^{-1}, \dots$  and  $q_{10}^{-1}$  with vibration frequency  $\omega$  for  $a = 50 \text{ nm}$  and  $a = 500 \text{ nm}$ , respectively. It is clear that for both the values of  $a = 50 \text{ nm}$  and  $a = 500 \text{ nm}$ , and throughout the investigated frequency range (i.e.  $10 \text{ MHz} \leq \omega \leq 10^7 \text{ MHz}$ ), the value of  $q_1^{-1}$  is greater than the values of  $q_2^{-1}$  to  $q_{10}^{-1}$  by a large distance, so that  $q_1^{-1}$  is at least  $10^4$  times  $q_{10}^{-1}$ . Based on this, it can be concluded that the terms of sequence  $q_j^{-1}$  are descending with a high rate.

Figure 4a shows the values of TED by taking into account the first, fifth, ninth and tenth terms of Eq. (51) (that is  $Q_1^{-1}, Q_5^{-1}, Q_9^{-1}$  and  $Q_{10}^{-1}$ ). In these diagrams, it is assumed that  $a = 50 \text{ nm}$ ,  $l_M = 0.5 \mu\text{m}$  and  $l_Q = 150 \text{ nm}$ . As it is clear, the difference of the results is so small that it

cannot be easily recognized from the figure. Moreover, the changes of ratio  $Q_n^{-1}/Q_{10}^{-1}$  for  $n = 1, 5$  and  $9$  with respect to vibration frequency  $\omega$  are portrayed in Fig. 4b. As can be seen, this ratio is greater than  $0.996$  for  $n = 1$  and is almost equal to one for  $n = 9$ . From this, it can be stated that accounting for the first ten terms of the relationship presented for TED (that is, the value of  $Q_{10}^{-1}$ ) can provide precise and convergent outcomes.

Figure 5 is similar to Fig. 4, with the only difference that it is drawn for a beam with cross-sectional radius  $a = 500 \text{ nm}$ . In Fig. 5a, it is apparent that at high frequencies, the value of  $Q_1^{-1}$  is somewhat lower than the values of  $Q_5^{-1}, Q_9^{-1}$  and  $Q_{10}^{-1}$ , although at low frequencies, the four mentioned values are almost identical. As can be readily seen in Fig. 5b, the values of  $Q_1^{-1}/Q_{10}^{-1}$  and  $Q_5^{-1}/Q_{10}^{-1}$  are greater than  $0.86$  and  $0.99$ , respectively. In addition, the value of  $Q_9^{-1}/Q_{10}^{-1}$  in the entire range under study for the vibration frequency  $\omega$  is almost equal to one. Hence, considering Figs. 4 and 5, it can be said that the inclusion of the first ten terms of Eq. (51), i.e. computing the amount of  $Q_{10}^{-1}$ , guarantees the convergence of the obtained result.



**Fig. 3** Variations of thermoelastic dissipation modes  $q_1^{-1}$ ,  $q_2^{-1}$ , ... and  $q_{10}^{-1}$  with vibration frequency  $\omega$  for **a**  $a = 50$  nm and **b**  $a = 500$  nm

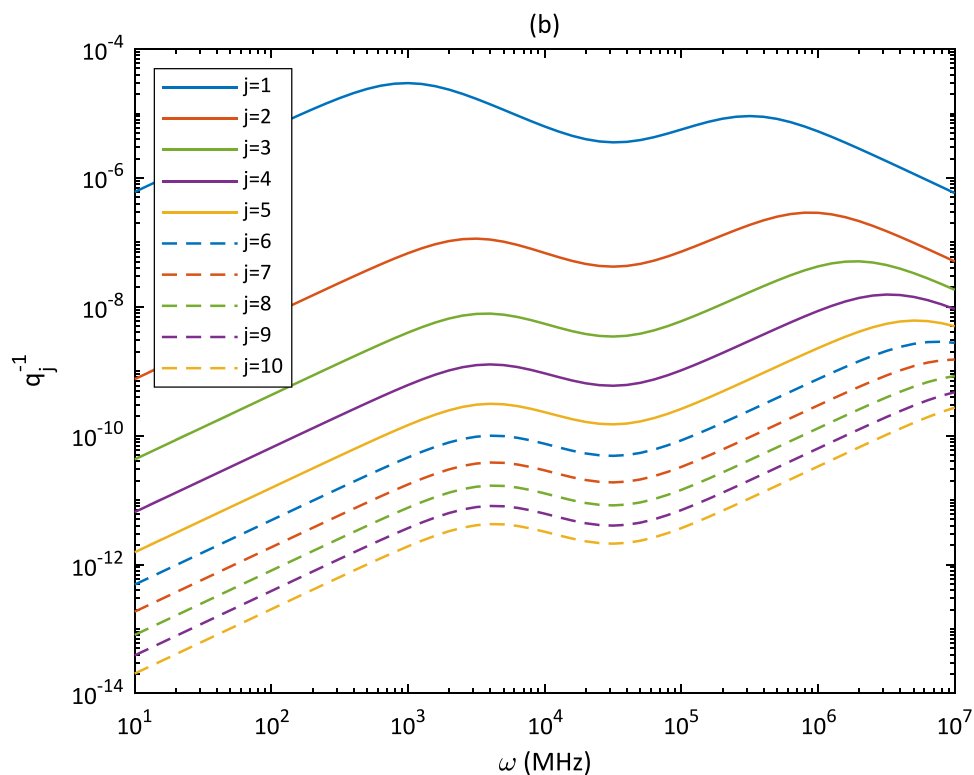
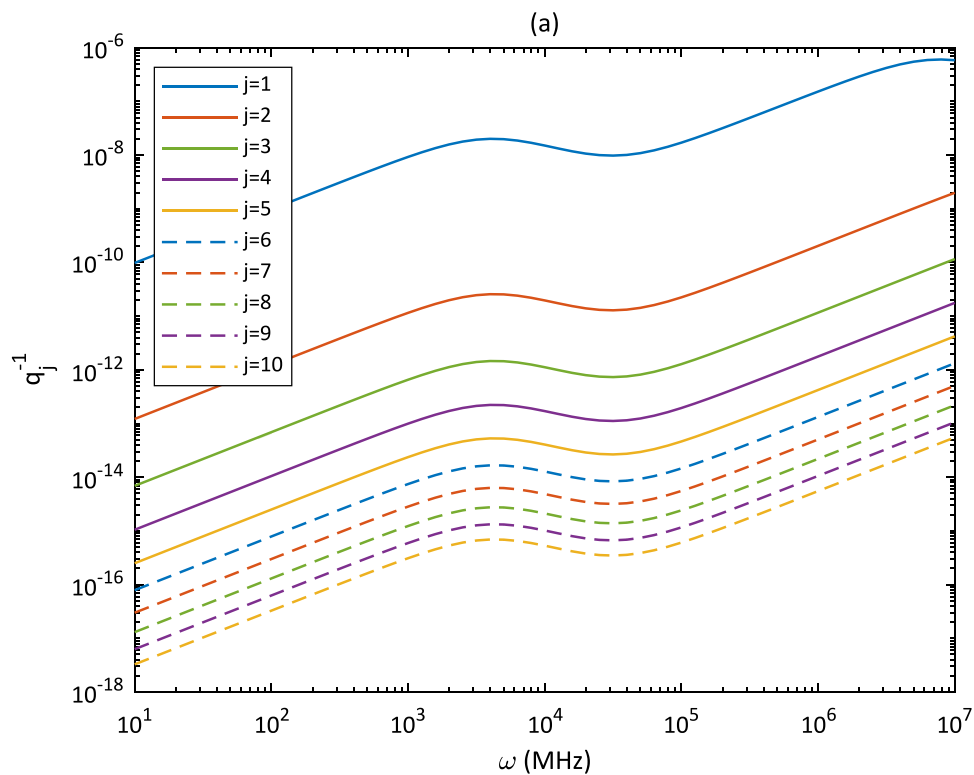
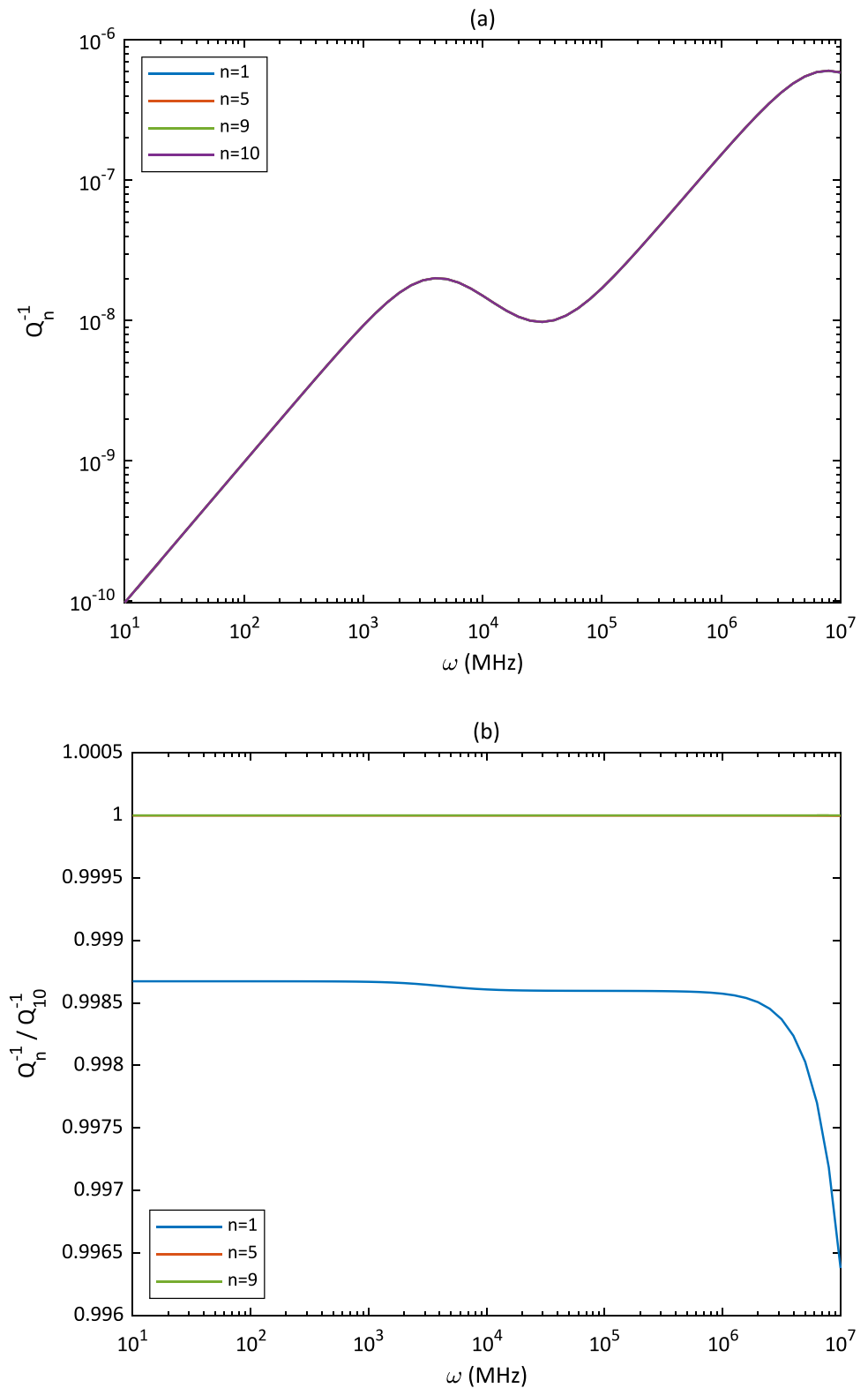


**Fig. 4** Convergence analysis for a beam with radius  $a = 50$  nm  
 (a)  $Q_1^{-1}$ ,  $Q_5^{-1}$ ,  $Q_9^{-1}$  and  $Q_{10}^{-1}$  (b)  $Q_n^{-1}/Q_{10}^{-1}$  for  $n = 1, 5$  and  $9$

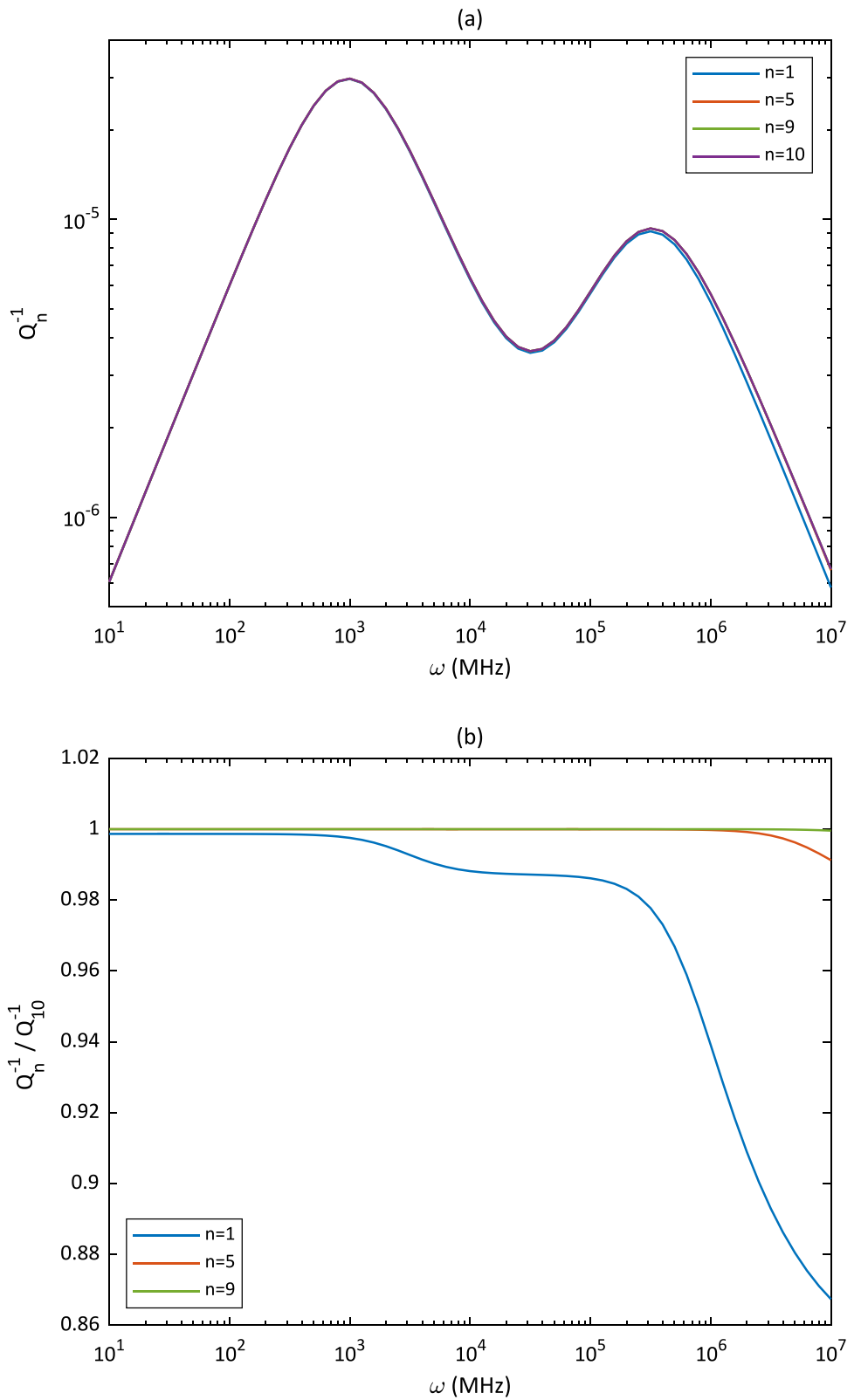


### Parametric Analysis

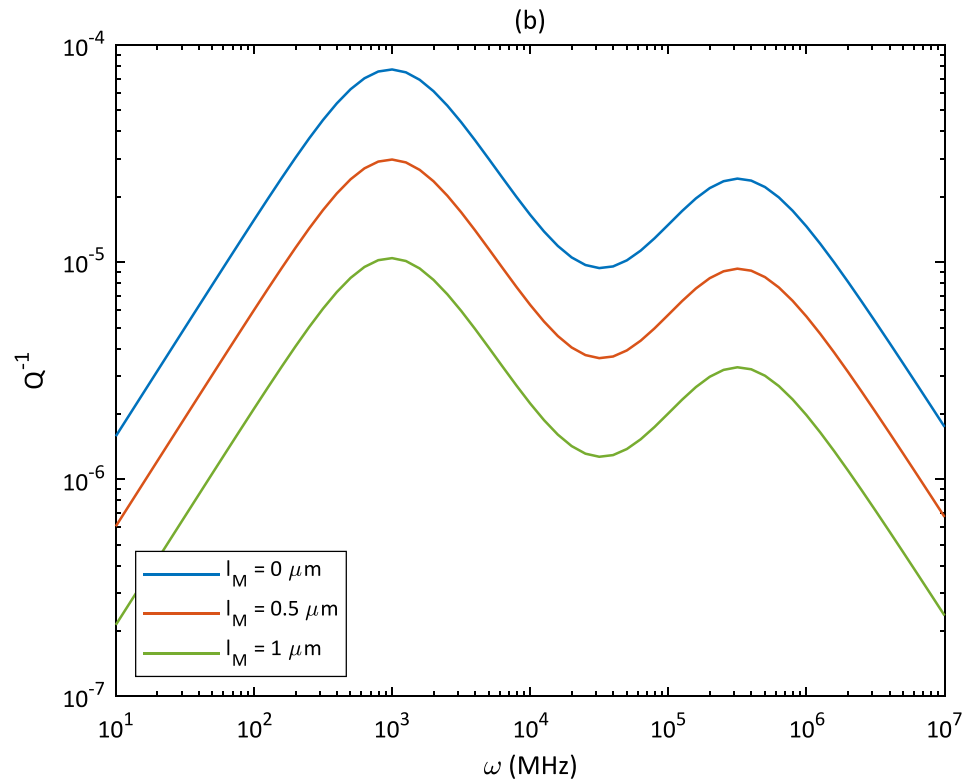
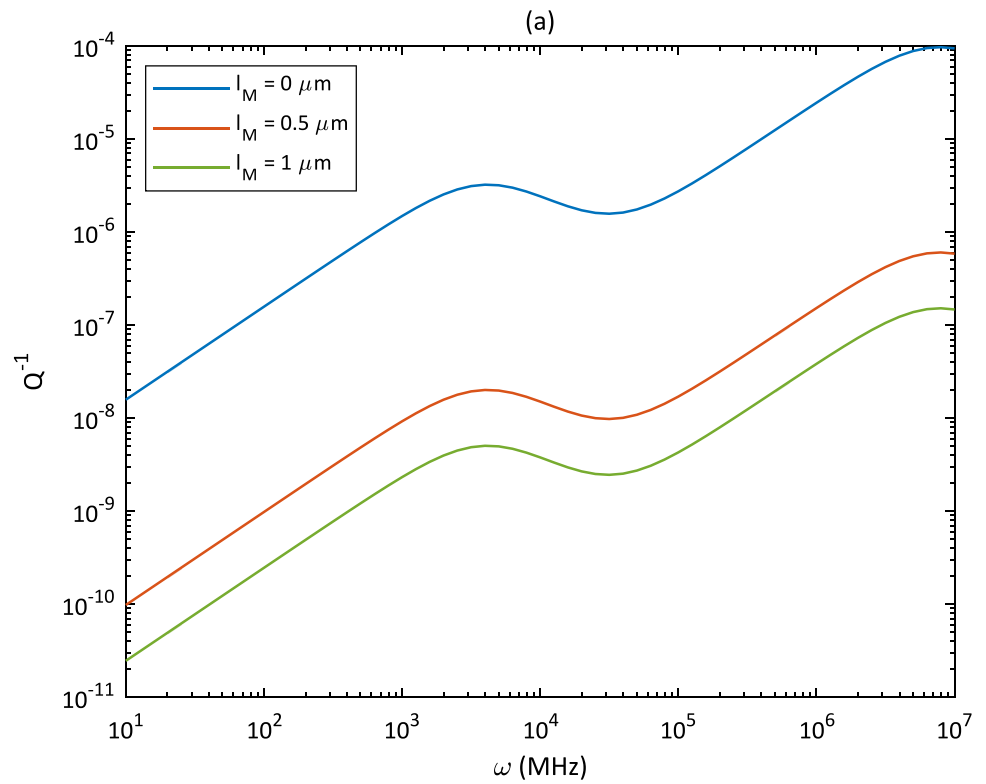
This section deals with the role of key factors such as the mechanical length scale parameter  $l_M$ , thermal nonlocal

parameter  $l_Q$ , beam size, reference temperature  $T_0$  and beam material in the amount and pattern of changes of TED. To this aim, except for the cases where the sensitivity of TED value to the material of the beam or reference temperature

**Fig. 5** Convergence analysis for a beam with radius  $a = 500\text{nm}$   
**a**  $Q_1^{-1}, Q_5^{-1}, Q_9^{-1}$  and  $Q_{10}^{-1}$  and **b**  $Q_n^{-1}/Q_{10}^{-1}$  for  $n = 1, 5$  and  $9$



**Fig. 6** Impact of mechanical length scale parameter  $l_M$  on TED variations with vibration frequency  $\omega$  **a**  $a = 50$  nm and **b**  $a = 500$  nm



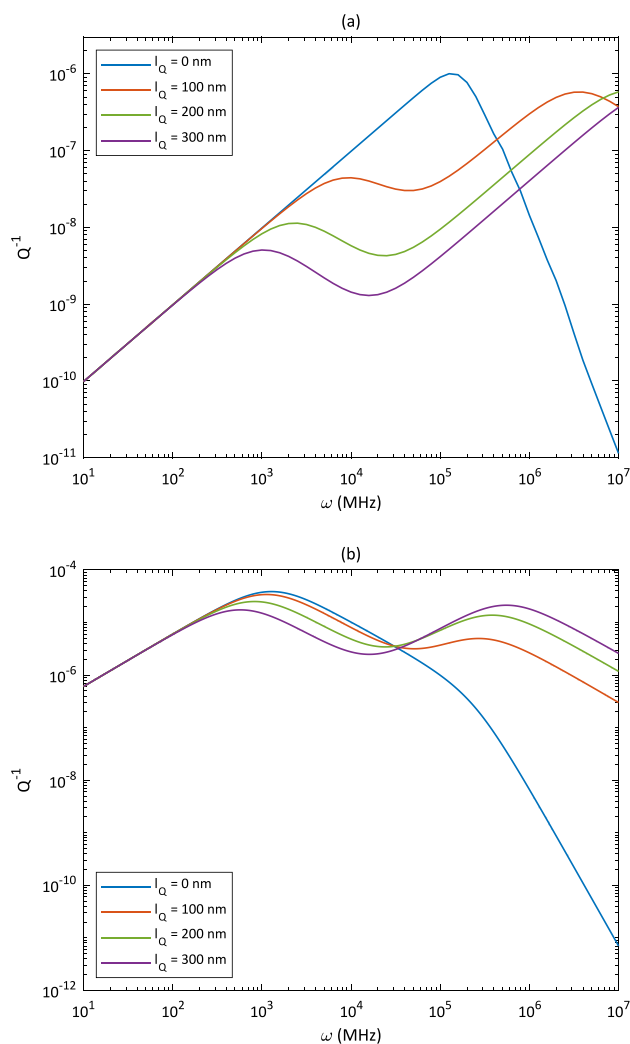


**Fig. 7** Impact of thermal nonlocal parameter  $l_Q$  on TED variations with vibration frequency  $\omega$  **a**  $a = 50$  nm and **b**  $a = 500$  nm

is investigated, a beam made of silicon at the reference temperature  $T_0 = 300$  K is considered.

In Fig. 6a and b, the impact of mechanical length scale parameter  $l_M$  on TED value is explored for beams with circular cross-sectional radius  $a = 50$  nm and  $a = 500$  nm, respectively. In these figures, the thermal nonlocal parameter is supposed to be  $l_Q = 150$  nm. As can be seen, for both the values adopted for the radius and throughout the considered interval for the vibration frequency, the larger value of  $l_M$  weakens TED. Another noteworthy point is that due to the larger radius in Fig. 6b, the impact of increasing the amount of  $l_M$  on TED value is reduced, providing further evidence for the reduction of size effect in bigger dimensions.

Figure 7 examines the influence of thermal nonlocal parameter  $l_Q$  on TED alterations against vibration frequency  $\omega$ . Figure 7a and b are plotted for a beam with geometric specifications  $a = 50$  nm and  $a = 500$  nm, respectively.

To extract these curves, it is assumed that  $l_M = 0.5$   $\mu\text{m}$ . According to the obtained results, at low frequencies (i.e.  $\omega < 100$  MHz), the effect of thermal nonlocal parameter on the amount of TED is trivial, and the difference between the predictions of SPL and NSPL models is imperceptible. At intermediate frequencies (i.e.  $100$  MHz  $< \omega < 5 \times 10^5$  MHz for  $a = 50$  nm, and  $100$  MHz  $< \omega < 5 \times 10^4$  MHz for  $a = 500$  nm), thermal nonlocal parameter attenuates TED value, but at high frequencies, this impact is reversed and TED value estimated by NSPL model gets higher than that anticipated by SPL model. Another thing that is evident in these figures is that the inclusion of thermal nonlocal parameter increases the number of peak points in TED curve, although the highest TED value occurred in the range under investigation of vibration frequency belongs to SPL model. Additionally, as expected, due to the larger dimensions of beam in Fig. 7b compared to Fig. 7a and the diminution of size effect, the difference between the estimates of NSPL and SPL models in Fig. 7b is smaller, especially at low and intermediate frequencies.

For different values of mechanical length scale parameter  $l_M$ , the variations of TED with the cross-sectional radius  $a$  are shown in Fig. 8. The amount of thermal nonlocal parameter is considered as  $l_Q = 150$  nm. According to the obtained results, regardless of the radius of the cross section of the beam, the higher the value of  $l_M$ , the smaller value is estimated for TED. It is also evident that as the radius enlarges, the disparity in TED values obtained for different values of  $l_M$  dwindles, which is relevant to the weakening of size-dependent behavior. Additionally, the comparison of Fig. 8a–d reveals that the influence of incorporating the couple stress effect is more pronounced at high frequencies compared to intermediate and low frequencies.

In Fig. 9, the dependency of TED value on radius  $a$  is appraised for different amounts of thermal nonlocal parameter  $l_Q$  and vibration frequency  $\omega$ . To obtain the results, it is supposed that  $l_M = 0.5$   $\mu\text{m}$ . As it can be seen, in lower frequencies (Fig. 9a and b), the inclusion of thermal nonlocal parameter leads to a diminution in TED value, but with increasing frequency (Fig. 9c), the reducing effect of  $l_Q$  on TED value weakens, and becomes an increasing effect at higher frequencies (Fig. 9d). In addition, in general, it can be said that for larger values of thermal nonlocal parameter, the value of the radius where the maximum TED value comes about enlarges.

Figure 10a and b exhibit the impact of temperature reference  $T_0$  on the variations of TED with vibration frequency for two cases  $a = 50$  nm and  $a = 500$  nm, respectively. To draw these figures, thermal nonlocal parameter  $l_Q$  is considered equal to 150 nm. Also, it is assumed that  $l_M = 0.5$   $\mu\text{m}$ . Thermomechanical properties of silicon at different temperatures are listed in Table 3 [90]. In general, it can be stated that with the increase of the reference

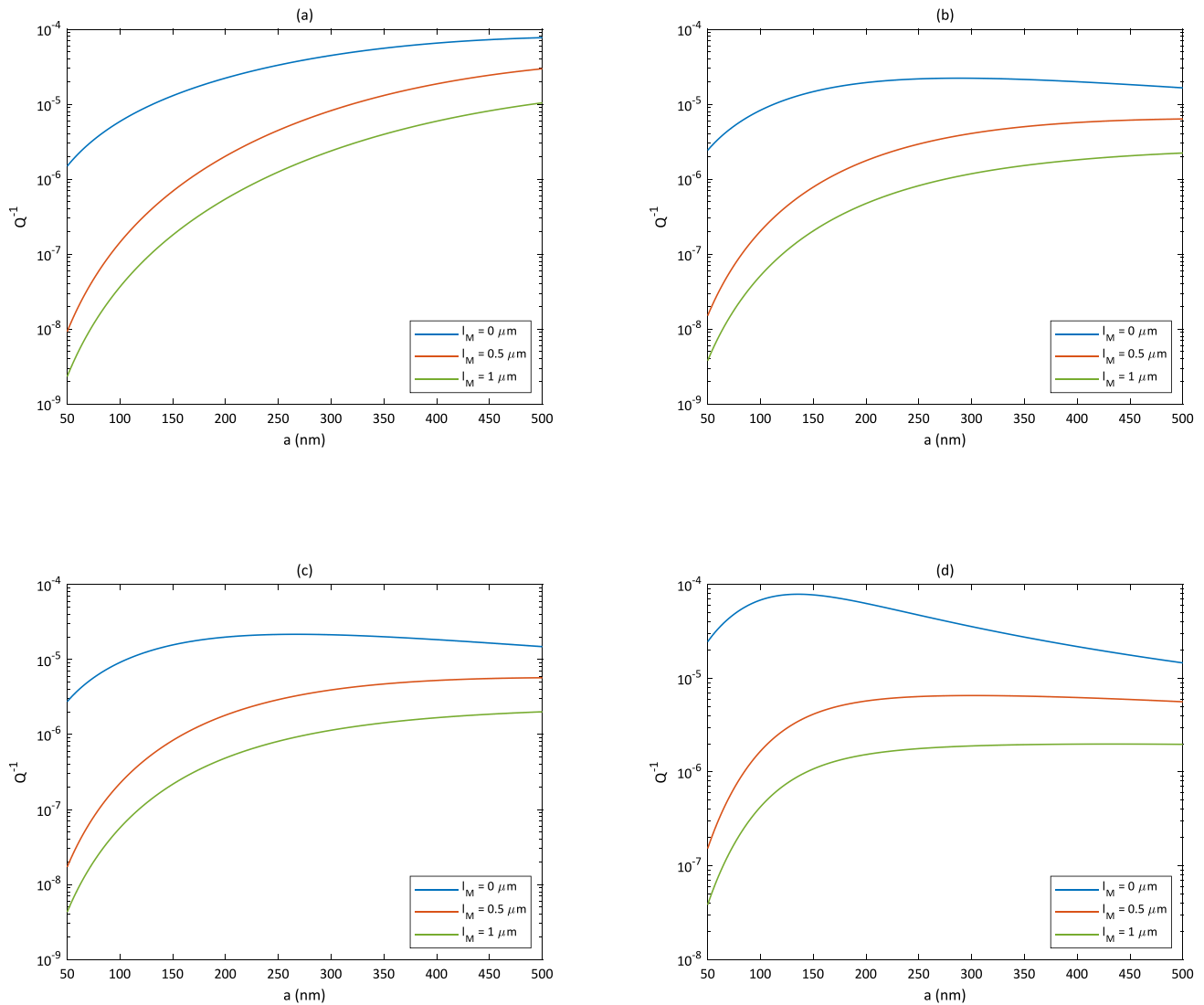


**Fig. 8** Sensitivity of TED value to radius  $a$  for different amounts of length scale parameter  $l_M$  **a**  $\omega = 10^3$  MHz, **b**  $\omega = 10^4$  MHz, **c**  $\omega = 10^5$  MHz and **d**  $\omega = 10^6$  MHz

temperature  $T_0$ , the value of TED enlarges, but it should be kept in mind that at the frequency where the highest TED value comes about at the reference temperature  $T_0 = 40$  K, the amount of TED computed for other temperatures is lower than that predicted for  $T_0 = 40$  K. It is also observed that with the increase of beam radius from 50 nm to 500 nm, the vibration frequency in which the maximum value of TED happens lessens for all reference temperatures. Moreover, at lower reference temperatures, TED peak points have a sharp appearance, but with the increase of  $T_0$ , TED curve becomes smoother at the peak points. It can also be seen that at the reference temperature  $T_0 = 40$  K, TED diagram has multiple peaks, but with increasing the value of  $T_0$ , TED curve tends to have one or two peak points.

To explore the influence of beam material on TED value, the variations of TED with respect to both the mechanical length scale parameter  $l_M$  and thermal nonlocal parameter  $l_Q$  are depicted in Figs. 11 and 12 for three materials silicon, gold and diamond. Thermomechanical properties of the mentioned materials at  $T_0 = 300$  K are presented in Table 2. Figures 11 and 12 correspond to vibration frequencies  $\omega = 10^3$  MHz and  $\omega = 10^6$  MHz, respectively. In addition, the surfaces presented in these figures are drawn for a beam with cross-sectional radius  $a = 300$  nm. Note that for a correct comparison between the calculated TED value for each material, the exact value of their mechanical length scale parameter  $l_M$  and thermal nonlocal parameter  $l_Q$  should be accessible. As it is clear, at lower frequency (i.e.  $\omega = 10^3$  MHz), regardless



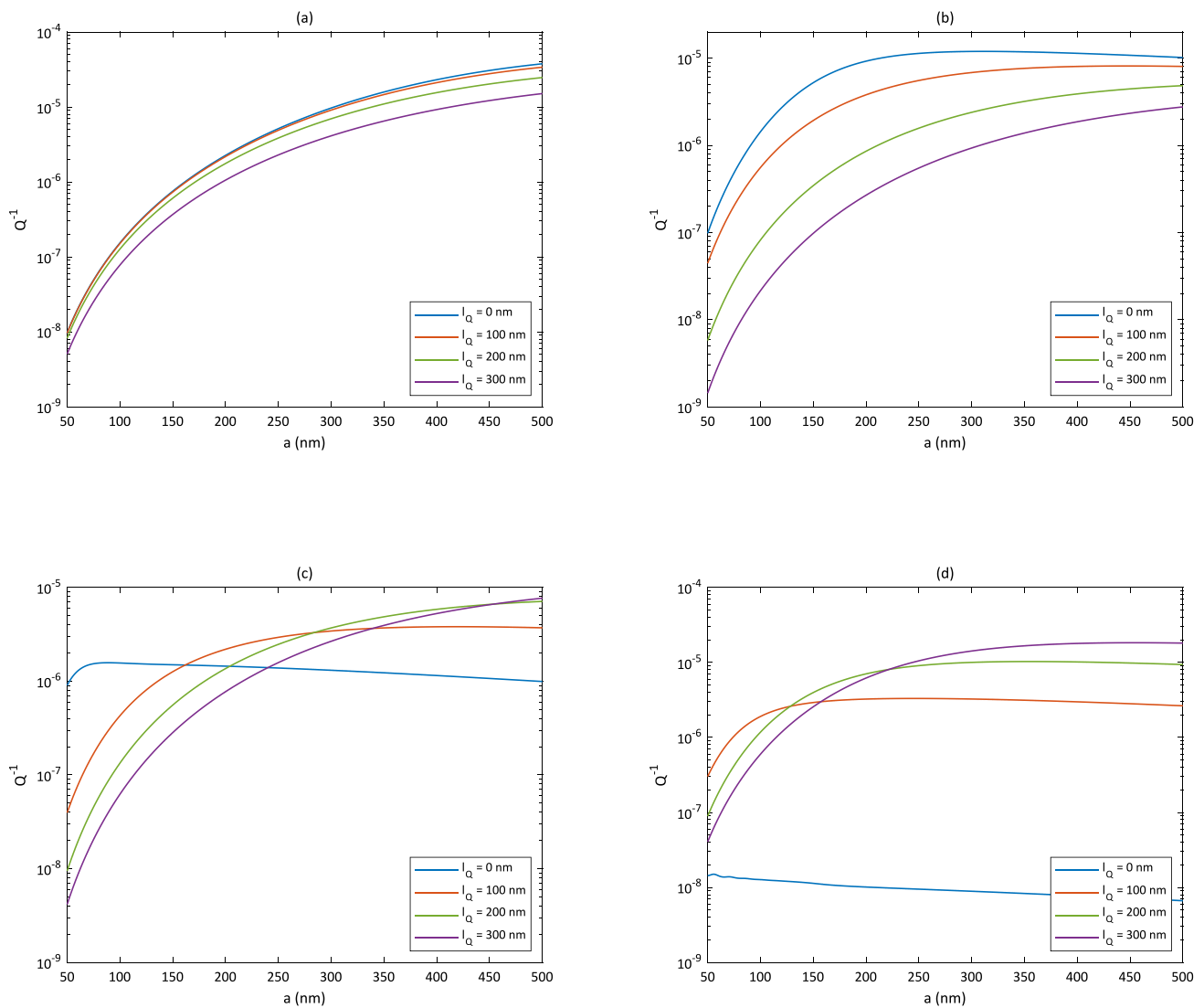


**Fig. 9** Sensitivity of TED value to radius  $a$  for different amounts of thermal nonlocal parameter  $l_Q$  **a**  $\omega = 10^3$  MHz, **b**  $\omega = 10^4$  MHz, **c**  $\omega = 10^5$  MHz and **d**  $\omega = 10^6$  MHz

of the actual amount of  $l_M$  and  $l_Q$  for the three studied materials, the highest value of TED belongs to golden beams, but at higher frequency (i.e.  $\omega = 10^6$  MHz), it is imperative to have information about the actual value of  $l_M$  and  $l_Q$  to compare the amounts of TED. As can be seen, regardless of the type of material or vibration frequency, increasing the amount of  $l_M$  attenuates TED value, but the influence of thermal nonlocal parameter  $l_Q$  (compared to SPL model) strongly depends on the vibration frequency  $\omega$  and type of material, in a way that can cause a decrease or increase in TED value compared to the estimation of the SPL model.

## Summary and Conclusions

In the paper at hand, the modified couple stress theory (MCST) and nonlocal single-phase-lag (NSPL) heat conduction model have been employed for the first time to provide a scale-dependent formulation for thermoelastic dissipation (TED) in circular cross-sectional micro/nano-beam resonators. In the first step, the NSPL-based heat conduction equation for Euler–Bernoulli beams with circular cross section has been derived in polar coordinates. By employing Bessel functions and solving the differential

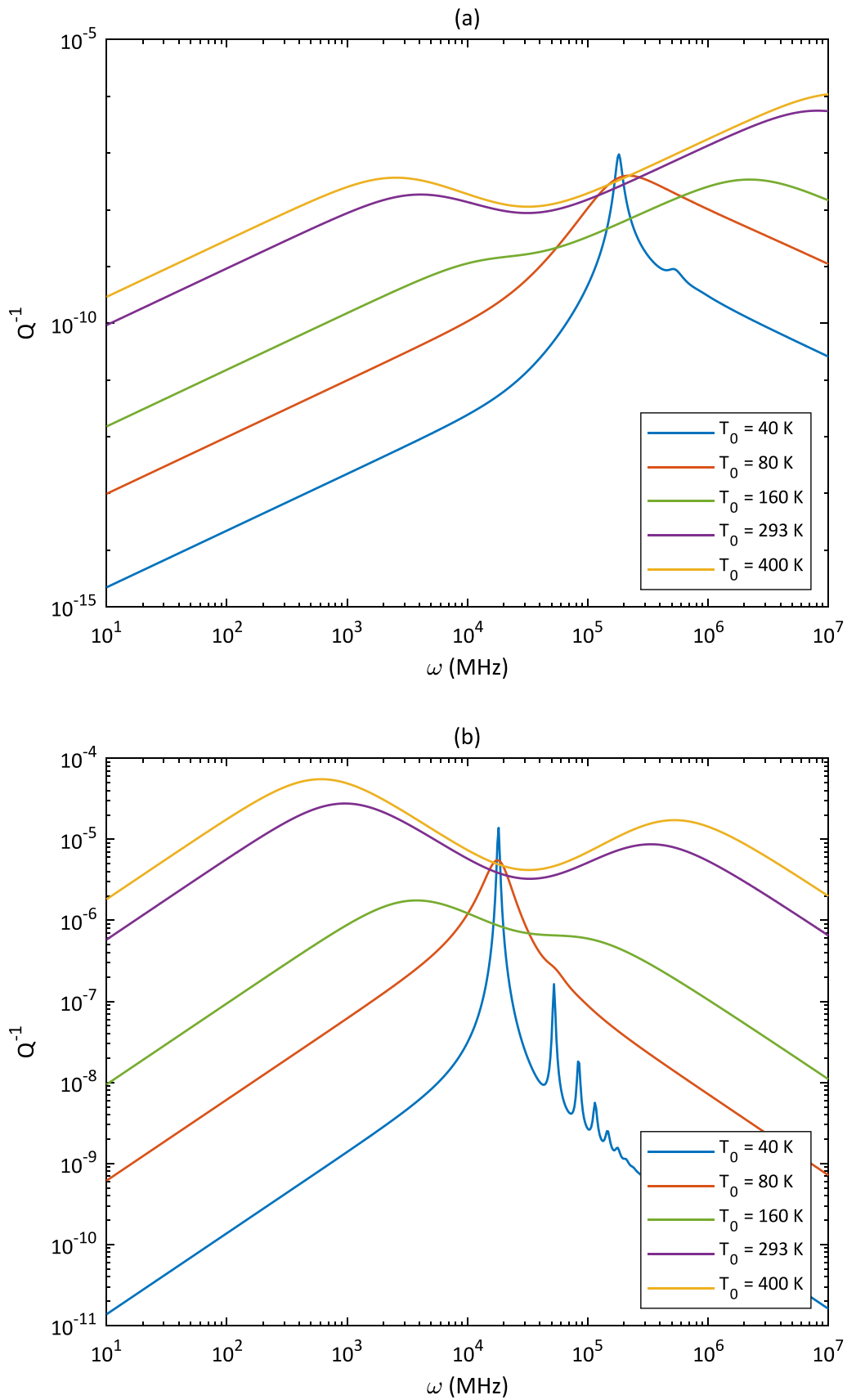


**Fig. 10** Influence of reference temperature  $T_0$  on the variations of TED with vibration frequency  $\omega$  for **a**  $a = 50$  nm and **b**  $a = 500$  nm

**Table 3** Mechanical and thermal constants of silicon at different reference temperatures

$T_0$ (K)	$E$ (GPa)	$\nu$	$\rho$ (kg/m <sup>3</sup> )	$k$ (W/mK)	$\rho c_v$ (J/m <sup>3</sup> K)	$\alpha$ (10 <sup>-6</sup> /K)	$\tau$ (ps)
40	169.3	0.22	2330	3660	$0.1 \times 10^6$	-0.164	1511.13
80	169.2	0.22	2330	1360	$0.4 \times 10^6$	-0.472	140.46
160	168.5	0.22	2330	375	$1.1 \times 10^6$	0.689	14.14
293	165.9	0.22	2330	156	$1.7 \times 10^6$	2.59	3.87
400	163.1	0.22	2327	105	$1.8 \times 10^6$	3.253	2.5

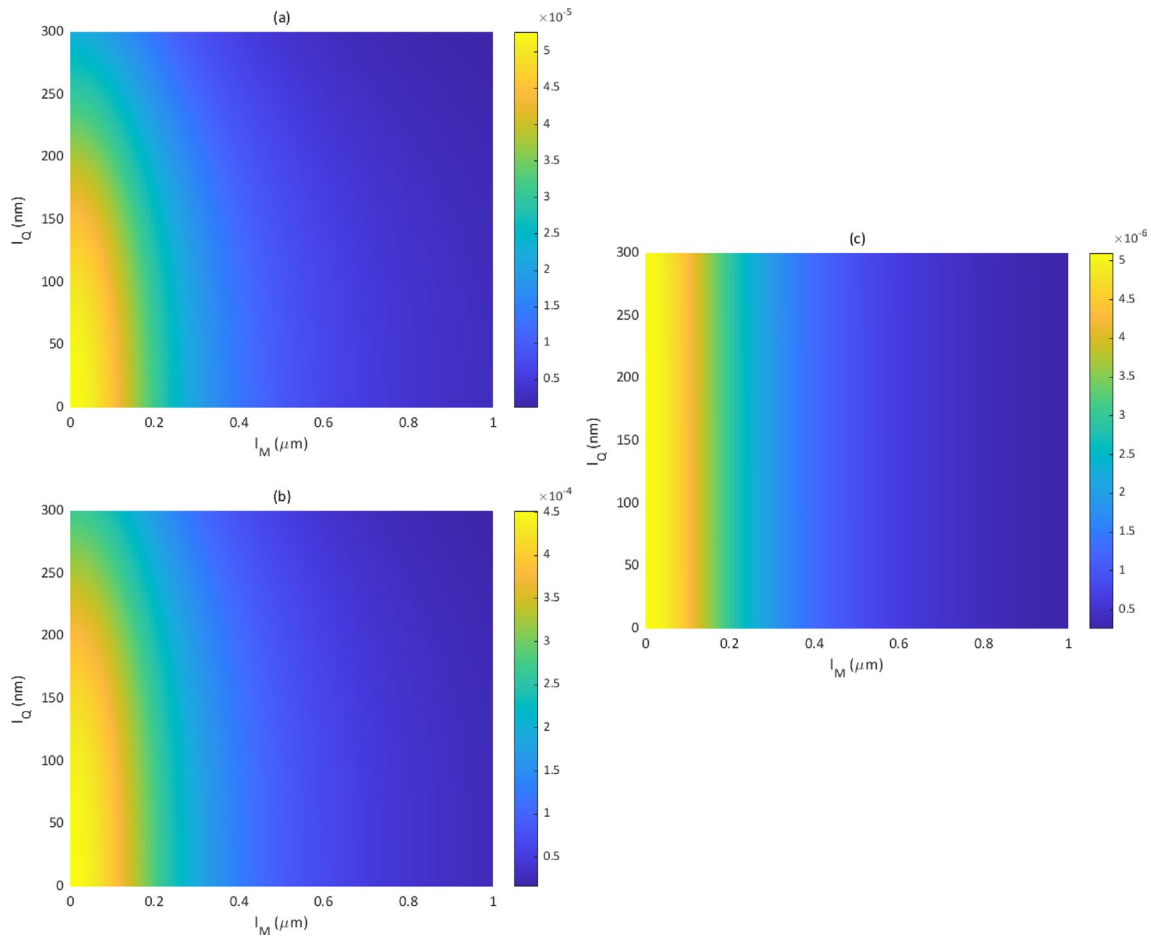


**Fig. 11** Effect of beam material on TED value for a beam with radius  $a = 300$  nm at vibration frequency  $\omega = 10^3$  MHz. **a** Silicon, **b** gold and **c** diamond

equation of heat, the temperature distribution in the beam has been specified. The classical and couple stress-based constitutive relations of the beam together with the extracted temperature field have been inserted in the relationship of TED according to the energy approach. In this way, a new TED expression has been rendered in the form of infinite series on the basis of MCST and NSPL model. The accuracy of the obtained solution has been assessed by way of a comparison study. By performing a convergence analysis, the requisite number of terms of TED relation for achieving accurate results has been determined. Also, via

an all-out parametric study, the influence of consequential factors such as the mechanical length scale parameter, thermal nonlocal parameter, cross-sectional radius of the beam, environment temperature and material type on TED has been scrutinized. The remarkable outcomes of this article are summarized below.

First, for all examined cross-sectional radii, vibration frequencies and materials, the inclusion of couple stress effect in the governing equations leads to a decrease in the TED value. Second, the increase of the ratio of beam radius to mechanical length scale parameter (i.e.  $a/l_M$ )

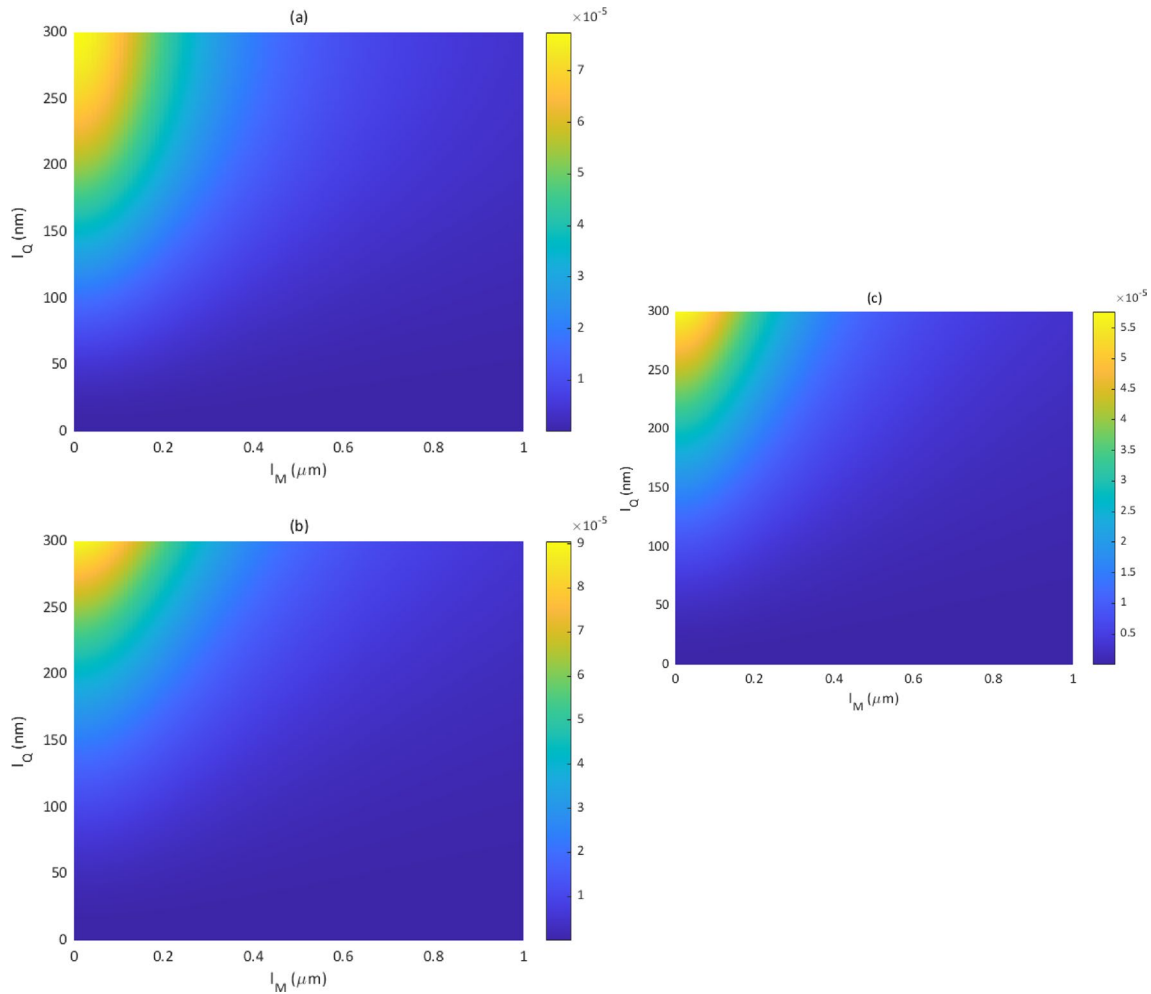


**Fig. 12** Effect of beam material on TED value for a beam with radius  $a = 300$  nm at vibration frequency  $\omega = 10^6$  MHz. **a** Silicon, **b** gold and **c** diamond

mitigates the impact of couple stress, so that TED value calculated based on the current formulation converges to the result of classical elasticity theory. Third, the effect of thermal nonlocal parameter  $l_Q$  on TED depends on the value of the vibration frequency, in such a way that at low frequencies (almost  $\omega < 100$  MHz) it does not make a significant difference compared to SPL model, at intermediate frequencies (approximately  $100 \text{ MHz} < \omega < 10^5 \text{ MHz}$ ) it causes a decrease in TED in comparison with SPL model and at high frequencies (about  $\omega > 10^5 \text{ MHz}$ ) it leads to TED amplification. Fourth, in general, for higher ambient temperatures, a higher value of TED is estimated. Fifth, at lower reference temperatures (more precisely at  $T_0 = 40 \text{ K}$ ), TED diagram exhibits multiple peaks. Sixth, regardless of the exact value of  $l_M$  and  $l_Q$ , at low frequencies (i.e.  $\omega = 10^3 \text{ MHz}$ ), among the three materials silicon, gold and diamond, beams made of gold experience the highest amount of TED, but at high frequencies ( $\omega = 10^6 \text{ MHz}$ ), for a valid comparison of TED value of

each of these materials, the exact amount of  $l_M$  and  $l_Q$  of each material should be available.

In a few words, it can be stated that if the characteristic lengths of beams with circular cross section, such as their cross-sectional radius, are within the range of mechanical length scale parameter or thermal nonlocal parameter, the impact of size must be included in the constitutive relations and heat equation. It is expected that due to the use of the modified couple stress theory (MCST) and nonlocal single-phase-lag (NSPL) model, the present work can help in the more accurate design of circular cross-sectional micro/nano-beam resonators.

**Data Availability** The raw data required to reproduce these findings can be accessed by directly contacting the corresponding author.

## Declarations

**Conflict of interest** There is no conflict of interest.

## References

1. Gao JY, Liu J, Yang HM, Liu HS, Zeng G, Huang B (2023) Anisotropic medium sensing controlled by bound states in the continuum in polarization independent metasurfaces. *Optics Express* 31(26):44703–44719
2. Wang YY, Lou M, Wang Y, Wu WG, Yang F (2022) Stochastic failure analysis of reinforced thermoplastic pipes under axial loading and internal pressure. *China Ocean Engineering* 36(4):614–628
3. Ding H, Chen LQ (2023) Shock isolation of an orthogonal six-DOFs platform with high-static-low-dynamic stiffness. *J Appl Mech* 90(11):111004–111001
4. Sun L, Liang T, Zhang C, Chen J (2023) The rheological performance of shearthickening fluids based on carbon fiber and silica nanocomposite. *Physics of Fluids* 35(3)
5. Lu Z, Yang T, Brennan MJ, Liu Z, Chen LQ (2017) Experimental investigation of a two-stage nonlinear vibration isolation system with high-static-low-dynamic stiffness. *Journal of Applied Mechanics* 84(2):021001
6. Wu S, Lin Q, Yuen Y, Tai YC (2001) MEMS flow sensors for nano-fluidic applications. *Sens Actuators A* 89(1–2):152–158
7. Ejeian F, Azadi S, Razmjou A, Orooji Y, Kottapalli A, Warkiani ME, Asadnia M (2019) Design and applications of MEMS flow sensors: a review. *Sens Actuators A* 295:483–502
8. Johnson BR, Cabuz E, French HB, Supino R (2010) Development of a MEMS gyroscope for northfinding applications. In: *IEEE/ION position, location and navigation symposium*, IEEE, pp 168–170
9. Koenig S, Rombach S, Gutmann W, Jaeckle A, Weber C, Ruf M, et al. (2019) Towards a navigation grade Si-MEMS gyroscope. In: *2019 DGON inertial sensors and systems (ISS)*, IEEE, pp 1–18
10. Senkal D, Shkel AM (2020) Whole-angle MEMS gyroscopes: challenges and opportunities. Wiley, Hoboken
11. Song P, Ma Z, Ma J, Yang L, Wei J, Zhao Y et al (2020) Recent progress of miniature MEMS pressure sensors. *Micromachines* 11(1):56
12. Zhang Y, Howver R, Gogoi B, Yazdi N (2011) A high-sensitive ultra-thin MEMS capacitive pressure sensor. In: *2011 16th International solid-state sensors, actuators and microsystems conference*. IEEE, pp 112–115
13. Xu R, Zhou S, Li WJ (2011) MEMS accelerometer based nonspecific-user hand gesture recognition. *IEEE Sens J* 12(5):1166–1173
14. Malayappan B, Lakshmi UP, Rao BP, Ramaswamy K, Pattnaik PK (2022) Sensing techniques and interrogation methods in optical mems accelerometers: a review. *IEEE Sens J* 22(7):6232–6246
15. Razzaghi MJP, Asadollahzadeh M, Tajbakhsh MR, Mohammadzadeh R, Abad MZM, Nadimi E (2023) Investigation of a temperature-sensitive ferrofluid to predict heat transfer and irreversibilities in LS-3 solar collector under line dipole magnetic field and a rotary twisted tape. *Int J Therm Sci* 185:108104
16. Mehdizadeh G, Nikoo MR, Talebbeydokhti N, Vanda S, Nematollahi B (2023) Hypolimnetic aeration optimization based on reservoir thermal stratification simulation. *J Hydrol* 625:130106
17. Ashraf MW, Tayyaba S, Afzulpurkar N (2011) Micro electro-mechanical systems (MEMS) based microfluidic devices for biomedical applications. *Int J Mol Sci* 12(6):3648–3704
18. Toupin RA (1964) Theories of elasticity with couple-stress. *Arch Ration Mech Anal* 17(2):85–112
19. Yang FACM, Chong ACM, Lam DCC, Tong P (2002) Couple stress based strain gradient theory for elasticity. *Int J Solids Struct* 39(10):2731–2743
20. Mindlin RD (1965) Second gradient of strain and surface-tension in linear elasticity. *Int J Solids Struct* 1(4):417–438
21. Lam DC, Yang F, Chong ACM, Wang J, Tong P (2003) Experiments and theory in strain gradient elasticity. *J Mech Phys Solids* 51(8):1477–1508
22. Eringen AC, Edelen D (1972) On nonlocal elasticity. *Int J Eng Sci* 10(3):233–248
23. Lim CW, Zhang G, Reddy J (2015) A higher-order nonlocal elasticity and strain gradient theory and its applications in wave propagation. *J Mech Phys Solids* 78:298–313
24. Sladek J, Sladek V, Hosseini SM (2021) Analysis of a curved Timoshenko nano-beam with flexoelectricity. *Acta Mech* 232:1563–1581
25. Jin H, Sui S, Zhu C, Li C (2023) Axial free vibration of rotating FG piezoelectric nano-rods accounting for nonlocal and strain gradient effects. *J Vib Eng Technol* 11(2):537–549
26. Sarparast H, Alibeigloo A, Borjalilou V, Koochakianfard O (2022) Forced and free vibrational analysis of viscoelastic nanotubes conveying fluid subjected to moving load in hygro-thermo-magnetic environments with surface effects. *Arch Civ Mech Eng* 22(4):172
27. Hosseini SM, Sladek J, Sladek V, Zhang C (2024) Effects of the strain gradients on the band structures of the elastic waves propagating in 1D phononic crystals: an analytical approach. *Thin-Walled Struct* 194:111316
28. Yapanmıř BE (2023) Nonlinear vibration and internal resonance analysis of microbeam with mass using the modified coupled stress theory. *J Vib Eng Technol* 11(5):2167–2180
29. Zheng F, Lu Y, Ebrahimi-Mamaghani A (2022) Dynamical stability of embedded spinning axially graded micro and nanotubes conveying fluid. *Waves Random Complex Media* 32(3):1385–1423
30. Sladek V, Sladek J, Repka M, Sator L (2020) FGM micro/nanoplates within modified couple stress elasticity. *Compos Struct* 245:112294
31. Panahi R, Asghari M, Borjalilou V (2023) Nonlinear forced vibration analysis of micro-rotating shaft–disk systems through a formulation based on the nonlocal strain gradient theory. *Arch Civ Mech Eng* 23(2):85
32. Qiu M, Lei D, Ou Z (2022) Nonlinear vibration analysis of fractional viscoelastic nanobeam. *J Vib Eng Technol* 11:4015–4038
33. Borjalilou V, Taati E, Ahmadian MT (2019) Bending, buckling and free vibration of nonlocal FG-carbon nanotube-reinforced composite nanobeams: exact solutions. *SN Appl Sci* 1:1–15
34. Sladek J, Sladek V, Wünsche M, Tan CL (2017) Crack analysis of size-dependent piezoelectric solids under a thermal load. *Eng Fract Mech* 182:187–201
35. Li J, Wang Z, Zhang S, Lin Y, Wang L, Sun C, Tan J (2023) A novelty mandrel supported thin-wall tube bending cross-section quality analysis: a diameter-adjustable multi-point contact mandrel. *The International Journal of Advanced Manufacturing Technology* 124(11):4615–4637
36. Wang Z, Zhou T, Zhang S, Sun C, Li J, Tan J (2023) Bo-LSTM based crosssectional profile sequence progressive prediction method for metal tube rotate draw bending. *Advanced Engineering Informatics* 58:102152
37. Shi X, Yang Y, Zhu X, Huang Z (2024) Stochastic dynamics analysis of the rocket shell coupling system with circular plate fasteners based on spectro-geometric method. *Composite Structures* 329:117727
38. Li M, Wang T, Chu F, Han Q, Qin Z, Zuo MJ (2020) Scaling-basis chirplet transform. *IEEE Transactions on Industrial Electronics* 68(9):8777–8788
39. Lord HW, Shulman Y (1967) A generalized dynamical theory of thermoelasticity. *J Mech Phys Solids* 15(5):299–309
40. Green AE, Naghdi P (1993) Thermoelasticity without energy dissipation. *J Elast* 31(3):189–208
41. Green AE, Lindsay K (1972) Thermoelasticity. *J Elast* 2(1):1–7

42. Quintanilla R (2019) Moore–Gibson–Thompson thermoelasticity. *Math Mech Solids* 24(12):4020–4031
43. Tzou DY (1995) The generalized lagging response in small-scale and high-rate heating. *Int J Heat Mass Transf* 38(17):3231–3240
44. Tzou DY, Guo ZY (2010) Nonlocal behavior in thermal lagging. *Int J Therm Sci* 49(7):1133–1137
45. Sladek J, Sladek V, Repka M, Pan E (2020) A novel gradient theory for thermoelectric material structures. *Int J Solids Struct* 206:292–303
46. Kazemi M, Rad MHG, Hosseini SM (2023) Geometrically non-linear vibration and coupled thermo-elasticity analysis with energy dissipation in fg multilayer cylinder reinforced by graphene platelets using MLPG method. *J Vib Eng Technol* 11(1):355–379
47. Liu D, Geng T, Wang H, Esmaili S (2023) Analytical solution for thermoelastic oscillations of nonlocal strain gradient nanobeams with dual-phase-lag heat conduction. *Mech Based Des Struct Mach* 51(9):4946–4976
48. Abouelregal AE, Moaaz O, Khalil KM, Abouhawwash M, Nasr ME (2023) A phase delay thermoelastic model with higher derivatives and two temperatures for the hall current effect on a micropolar rotating material. *J Vib Eng Technol* 12:1505–1523
49. Yue X, Yue X, Borjalilou V (2021) Generalized thermoelasticity model of nonlocal strain gradient Timoshenko nanobeams. *Arch Civ Mech Eng* 21(3):124
50. Hosseini SM, Sladek J, Sladek V (2020) Nonlocal coupled photo-thermoelasticity analysis in a semiconducting micro/nano beam resonator subjected to plasma shock loading: a Green-Naghdi-based analytical solution. *Appl Math Model* 88:631–651
51. Kadian P, Kumar S, Sangwan M (2023) Effect of inclined mechanical load on a rotating microelongated two temperature thermoelastic half space with temperature dependent properties. *J Vib Eng Technol*. <https://doi.org/10.1007/s42417-023-01105-1>
52. Yu JN, She C, Xu YP, Esmaili S (2022) On size-dependent generalized thermoelasticity of nanobeams. *Waves Random Complex Media*. <https://doi.org/10.1080/17455030.2021.2019351>
53. Ali BM, Batoor KM, Hussain S, Hussain W, Khazaal WM, Mohammed BA et al (2023) Scale-dependent generalized thermoelastic damping in vibrations of small-sized rectangular plate resonators by considering three-dimensional heat conduction. *Int J Struct Stab Dyn*. <https://doi.org/10.1142/S0219455424502225>
54. Sharma DK, Bachher M, Sharma MK, Sarkar N (2021) On the analysis of free vibrations of nonlocal elastic sphere of FGM type in generalized thermoelasticity. *Journal of Vibration Engineering & Technologies* 9:149–160
55. Singh B, Mukhopadhyay S (2023) Thermoelastic vibration of Timoshenko beam under the modified couple stress theory and the Moore–Gibson–Thompson heat conduction model. *Math Mech Solids*. <https://doi.org/10.1177/10812865231186127>
56. Abouelregal AE, Akgöz B, Civalek Ö (2022) Nonlocal thermoelastic vibration of a solid medium subjected to a pulsed heat flux via Caputo-Fabrizio fractional derivative heat conduction. *Appl Phys A* 128(8):660
57. Gu B, He T (2021) Investigation of thermoelastic wave propagation in Euler-Bernoulli beam via nonlocal strain gradient elasticity and GN theory. *J Vib Eng Technol* 9:715–724
58. Kharnoob MM, Cepeda LC, Jácome E, Choto S, Abdulally Abdulhussien Alazbjee A, Sapaev IB et al (2023) Analysis of thermoelastic damping in a microbeam following a modified strain gradient theory and the Moore–Gibson–Thompson heat equation. *Mech Time-Depend Mater*. <https://doi.org/10.1007/s11043-023-09632-w>
59. Weng W, Lu Y, Borjalilou V (2021) Size-dependent thermoelastic vibrations of Timoshenko nanobeams by taking into account dual-phase-lagging effect. *Eur Phys Jo Plus* 136:1–26
60. Pathania V, Dhiman P (2023) Generalized poro-thermoelastic waves in the cylindrical plate framed with liquid layers. *J Vib Eng Technol* 12:953–969
61. Zener C (1937) Internal friction in solids. I. Theory of internal friction in reeds. *Phys Rev* 52(3):230
62. Lifshitz R, Roukes ML (2000) Thermoelastic damping in micro- and nanomechanical systems. *Phys Rev B* 61(8):5600
63. Guo FL, Wang GQ, Rogerson G (2012) Analysis of thermoelastic damping in micro- and nanomechanical resonators based on dual-phase-lagging generalized thermoelasticity theory. *Int J Eng Sci* 60:59–65
64. Zhou H, Li P, Fang Y (2018) Thermoelastic damping in circular cross-section micro/nanobeam resonators with single-phase-lag time. *Int J Mech Sci* 142:583–594
65. Zhou H, Li P, Zuo W, Fang Y (2020) Dual-phase-lag thermoelastic damping models for micro/nanobeam resonators. *Appl Math Model* 79:31–51
66. Zuo W, Li P, Du J, Tse ZTH (2022) Thermoelastic damping in anisotropic piezoelectric microbeam resonators. *Int J Heat Mass Transf* 199:123493
67. Kim JH, Kim JH (2023) Dual-phase-lagging thermoelastic dissipation for toroidal micro/nano-ring resonator model. *Therm Sci Eng Progr* 39:101683
68. Zheng L, Wu Z, Wen S, Li F (2023) Thermoelastic damping in cylindrical shells with arbitrary boundaries. *Int J Heat Mass Transf* 206:123948
69. Kumar H, Mukhopadhyay S (2023) Size-dependent thermoelastic damping analysis in nanobeam resonators based on Eringen's nonlocal elasticity and modified couple stress theories. *J Vib Control* 29(7–8):1510–1523
70. Shi S, He T, Jin F (2021) Thermoelastic damping analysis of size-dependent nano-resonators considering dual-phase-lag heat conduction model and surface effect. *Int J Heat Mass Transf* 170:120977
71. Borjalilou V, Asghari M (2018) Small-scale analysis of plates with thermoelastic damping based on the modified couple stress theory and the dual-phase-lag heat conduction model. *Acta Mech* 229:3869–3884
72. Yang L, Li P, Gao Q, Gao T (2022) Thermoelastic damping in rectangular micro/nanoplate resonators by considering three-dimensional heat conduction and modified couple stress theory. *J Therm Stress* 45(11):843–864
73. Ge Y, Sarkar A (2023) Thermoelastic damping in vibrations of small-scaled rings with rectangular cross-section by considering size effect on both structural and thermal domains. *Int J Struct Stab Dyn* 23(03):2350026
74. Kakhki EK, Hosseini SM, Tahani M (2016) An analytical solution for thermoelastic damping in a micro-beam based on generalized theory of thermoelasticity and modified couple stress theory. *Appl Math Model* 40(4):3164–3174
75. Jalil AT, Karim N, Ruhaima AAK, Sulaiman JMA, Hameed AS, Abed AS et al (2023) Analytical model for thermoelastic damping in in-plane vibrations of circular cross-sectional micro/nanorings with dual-phase-lag heat conduction. *J Vib Eng Technol* 11:1391
76. Weng L, Xu F, Chen X (2024) Three-dimensional analysis of thermoelastic damping in couple stress-based rectangular plates with nonlocal dual-phase-lag heat conduction. *Eur J Mech A/Solids* 105:105223
77. Borjalilou V, Asghari M, Bagheri E (2019) Small-scale thermoelastic damping in micro-beams utilizing the modified couple stress theory and the dual-phase-lag heat conduction model. *J Therm Stress* 42(7):801–814
78. Li F, Esmaili S (2021) On thermoelastic damping in axisymmetric vibrations of circular nanoplates: incorporation of size effect into structural and thermal areas. *Eur Phys J Plus* 136(2):1–17



79. Chugh N, Partap G (2021) Study of thermoelastic damping in microstretch thermoelastic thin circular plate. *J Vib Eng Technol* 9:105–114
80. Al-Hawary SIS, Huamán-Romaní YL, Sharma MK, Kuaquira-Huallpa F, Pant R, Romero-Parra RM et al (2024) Non-Fourier thermoelastic damping in small-sized ring resonators with circular cross section according to Moore–Gibson–Thompson generalized thermoelasticity theory. *Arch Appl Mech* 94:469–491
81. Kim JH, Kim JH (2019) Phase-lagging of the thermoelastic dissipation for a tubular shell model. *Int J Mech Sci* 163:105094
82. Yani A, Abdullaev S, Alhassan MS, Sivaraman R, Jalil AT (2023) A non-Fourier and couple stress-based model for thermoelastic dissipation in circular microplates according to complex frequency approach. *Int J Mech Mater Des* 19:645–668
83. Li M, Cai Y, Fan R, Wang H, Borjalilou V (2022) Generalized thermoelasticity model for thermoelastic damping in asymmetric vibrations of nonlocal tubular shells. *Thin-Walled Struct* 174:109142
84. Odira I, Byiringiro J, Keraita J (2023) Probing multimode thermoelastic damping in MEMS beam mass structure. *J Vib Eng Technol*. <https://doi.org/10.1007/s42417-023-01137-7>
85. Hai L, Kim DJ (2023) Nonlocal dual-phase-lag thermoelastic damping in small-sized circular cross-sectional ring resonators. *Mech Adv Mater Struct*. <https://doi.org/10.1080/15376494.2023.2245822>
86. Al-Bahrani M, AbdulAmeer SA, Yasin Y, Alanssari AI, Hameed AS, Sulaiman JMA et al (2023) Couple stress-based thermoelastic damping in microrings with rectangular cross section according to Moore–Gibson–Thompson heat equation. *Arch Civ Mech Eng* 23(3):151
87. Jalil AT, Saleh ZM, Imran AF, Yasin Y, Ruhaima AAK, Gatea MA, Esmaili S (2023) A size-dependent generalized thermoelasticity theory for thermoelastic damping in vibrations of nanobeam resonators. *Int J Struct Stab Dyn* 23:2350133
88. Zhao G, Shi S, Gu B, He T (2021) Thermoelastic damping analysis to nano-resonators utilizing the modified couple stress theory and the memory-dependent heat conduction model. *J Vib Eng Technol* 10:715–726
89. Borjalilou V, Asghari M, Taati E (2020) Thermoelastic damping in nonlocal nanobeams considering dual-phase-lagging effect. *J Vib Control* 26(11–12):1042–1053
90. Zhou H, Li P, Fang Y (2019) Single-phase-lag thermoelastic damping models for rectangular cross-sectional micro-and nano-ring resonators. *Int J Mech Sci* 163:105132

**Publisher's Note** Springer Nature remains neutral with regard to jurisdictional claims in published maps and institutional affiliations.

Springer Nature or its licensor (e.g. a society or other partner) holds exclusive rights to this article under a publishing agreement with the author(s) or other rightsholder(s); author self-archiving of the accepted manuscript version of this article is solely governed by the terms of such publishing agreement and applicable law.

## Authors and Affiliations

Younus Fahad Breesam<sup>1</sup> · Sherzod Shukhratovich Abdullaev<sup>2,3</sup> · Raed H. Althomali<sup>4</sup> · F. Al-dolaimy<sup>5</sup> · M. K. Sharma<sup>6</sup> · Muataz S. Alhassan<sup>7</sup> · Ahmed Hussien Alawadi<sup>10,8,9</sup> · Ali Alsaalamy<sup>11</sup> · Kadhim Abbas Jabbar<sup>12</sup>

✉ Sherzod Shukhratovich Abdullaev  
sherzodbek.abdullaev.1001@gmail.com

Younus Fahad Breesam  
Younus.fahad@mtu.edu.iq

<sup>1</sup> Department of Mechanical Techniques, Technical Instructors Training Institute, Middle Technical University, Baghdad, Iraq

<sup>2</sup> Faculty of Chemical Engineering, New Uzbekistan University, Tashkent, Uzbekistan

<sup>3</sup> Department of Science and Innovation, Tashkent State Pedagogical University Named After Nizami, Tashkent, Uzbekistan

<sup>4</sup> Department of Chemistry, College of Science and Humanities in Al-Kharj, Prince Sattam Bin Abdulaziz University, Al-Kharj 11942, Saudi Arabia

<sup>5</sup> Al-Zahraa University for Women, Karbala, Iraq

<sup>6</sup> Department of Mathematics, Chaudhary Charan Singh University, Meerut 250004, Uttar Pradesh, India

<sup>7</sup> Division of Advanced Nano Material Technologies, Scientific Research Center, Al-Ayen University, Thi-Qar, Iraq

<sup>8</sup> College of Technical Engineering, The Islamic University, Najaf, Iraq

<sup>9</sup> College of Technical Engineering, The Islamic University of Al Diwaniyah, Al-Qadisiyyah, Iraq

<sup>10</sup> College of Technical Engineering, The Islamic University of Babylon, Babylon, Iraq

<sup>11</sup> College of Technical Engineering, Imam Ja'afar Al-Sadiq University, Al-Muthanna 66002, Iraq

<sup>12</sup> Technical Engineering College, National University of Science and Technology, Dhi Qar, Iraq